1 **The SERM/SERD Bazedoxifene Disrupts ESR1 Helix 12 to Overcome Acquired Hormone**
2 **Resistance in Breast Cancer Cells**

3 Sean W. Fanning[1], Rinath Jeselsohn[2,3], Venkatasubramanian Dharmarajan[4], Christopher G. Mayne[5,6],
4 Mostafa Karimi[7], Gilles Buchwalter[2], Rene Houtman[8], Weiyi Toy[9], Colin E. Fowler[1], Muriel Lainé[1],
5 Kathryn E Carlson[5], Teresa A. Martin[5], Jason Nowak[4], Jerome Nwachukwu[4], David J. Hosfield[1], Sarat
6 Chandarlapaty[9], Emad Tajkhorshid[6], Kendall W. Nettles[4], Patrick R. Griffin[4], Yang Shen[7], John A.
7 Katzenellenbogen[5], Myles Brown[2,3], Geoffrey L. Greene[1]
8
9 1: Ben May Department for Cancer Research, University of Chicago, Chicago, IL 60637 USA
10 2: Center for Functional Cancer Epigenetics, Dana-Farber Cancer Institute, Boston, MA 02215 USA
11 3: Department of Medical Oncology, Dana Farber Cancer Institute, Boston, MA 02215 USA
12 4. Department of Molecular Medicine, The Scripps Research Institute, Jupiter, FL 33458, USA
13 5: Department of Chemistry, University of Illinois at Urbana-Champaign, Urbana, IL 61801 USA
14 6: Department of Biochemistry, College of Medicine, Center for Biophysics and Computational Biology,
15 and Beckman Institute for Advanced Science and Technology, University of Illinois at Urbana-
16 Champaign, Urbana, IL 61801 USA
17 7: Department of Electrical and Computer Engineering, TEES-AgriLife Center for Bioinformatics and
18 Genomic Systems Engineering, Texas A&M University, College Station, TX 77843 USA
19 8. PamGene International B.V, 's-Hertogenbosch, Netherlands 5211
20 9: Human Oncology and Pathogenesis Program, Memorial Sloan-Kettering Cancer Center (MSKCC),
21 New York, NY 10065, USA

22 **Running Title:** Bazedoxifene inhibits ERα with activating mutations.

23 **Precis:** Bazedoxifene's SERD activities enable it to resist the impact of activating ESR1
24 mutations.

25 **Keywords (5)**: ESR1 Somatic Mutations, Breast Cancer

26 **Significance:** Bazedoxifene (BZA) is a potent orally available antiestrogen that is clinically
27 approved for use in hormone replacement therapy (DUAVEE). We explore the efficacy of BZA
28 to inhibit activating somatic mutants of ERα that can arise in metastatic breast cancers after
29 prolonged exposure to aromatase inhibitors or tamoxifen therapy. Breast cancer cell line,
30 biophysical, and structural data show that BZA disrupts helix 12 of the ERα ligand binding
31 domain to achieve improved potency against Y537S and D538G somatic mutants compared to 4-
32 hydroxytamoxifen.

40 **Conflicts of Interest:** Giles Buchwalter is an employee and shareholder at Celgene. Rene
41 Houtman is an employee at PamGene International.

42 # Abstract

43 Acquired resistance to endocrine therapy remains a significant clinical burden for breast cancer

44 patients. Somatic mutations in the *ESR1* (estrogen receptor alpha (ERα) gene ligand-binding

45 domain (LBD) represent a recognized mechanism of acquired resistance. Antiestrogens with

46 improved efficacy versus tamoxifen might overcome the resistant phenotype in ER+ breast

47 cancers. Bazedoxifene (BZA) is a potent antiestrogen that is clinically approved for use in

48 hormone replacement therapies. We find BZA possesses improved inhibitory potency against the

49 Y537S and D538G ERα mutants compared to tamoxifen and has additional inhibitory activity in

50 combination with the CDK4/6 inhibitor palbociclib. In addition, comprehensive biophysical and

51 structural biology studies show that BZA's selective estrogen receptor degrading (SERD)

52 properties that override the stabilizing effects of the Y537S and D538G ERα mutations.

53

54

55

56

57

58

59

60

61

Introduction

63   Estrogen receptor alpha (ERα) plays critical roles in the etiology, treatment and

64 prevention of the majority of breast cancers [1]. Due to the high degree of efficacy and wide

65 therapeutic indices of endocrine therapies, patients may receive such treatments for progressive

66 disease over the course of several years [2]. Unfortunately, the majority of ER+ metastatic breast

67 cancers that initially respond to endocrine treatment will become refractory despite continued

68 ERα expression [2]. Selective estrogen receptor modulators (SERMs) like tamoxifen are

69 antagonistic in the breast and agonistic in the bone and endometrium. SERM agonist activity

70 stems from tissue-specific co-regulator binding in the presence of tamoxifen [3]. In addition,

71 somatic mutations to *ESR1* (gene for ERα) ligand binding domain (LBD) were identified in 25-

72 30% of patients who previously received endocrine treatment [2, 4-6]. Y537S and D538G are the

73 two most prevalent mutations, and pre-clinical studies show that these mutations confer

74 hormone-free transcriptional activity and relative resistance to tamoxifen and fulvestrant

75 treatment [2, 4-6]. Both mutants enable constitutive ERα activity by favoring the agonist-like

76 conformation of the receptor activating function-2 (AF-2) surface and significantly reduce

77 hormone and 4-hydroxytamoxifen (the active metabolite of tamoxifen) binding affinities [7, 8].

78   Endocrine treatments with improved efficacy could potentially overcome resistance

79 engendered by the activating somatic mutants and other mechanisms. In pre-clinical studies,

80 fulvestrant (FULV, a selective estrogen receptor degrader (SERD) and complete antiestrogen) at

81 high concentrations was the only molecule that reduced the Y537S and D538G ERα mutant

82 transcriptional activity to basal levels [2, 4-6]. However, its clinical efficacy is limited by poor
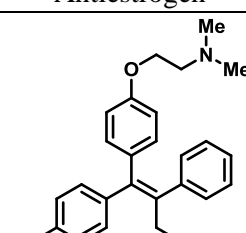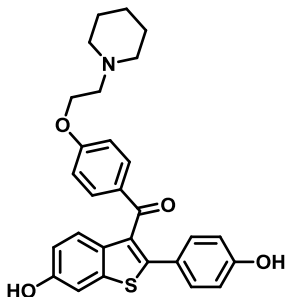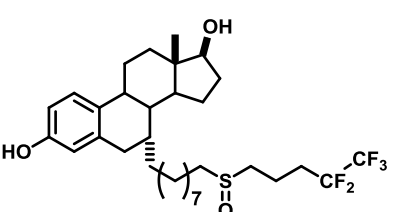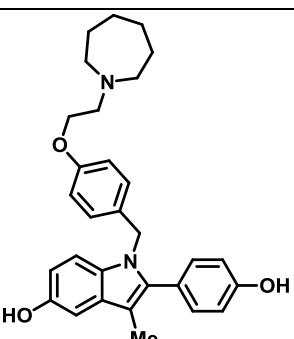
83   solubility and oral bioavailability [9-11]. Consequently, new complete antiestrogens with

84   improved oral bioavailability and pharmacokinetics, including AZD9496, GDC-0927, and

85   RAD1901, are currently in development, although their suitability as long-term endocrine

86   therapies remains to be determined [10, 12-14].

87   Here, we explore whether bazedoxifene (BZA), a potent antiestrogen that retains some

88   SERM properties, shows activity against breast cancer cells that express ESR1 somatic mutants.

89   We chose BZA because it has been extensively studied in clinical trials and is approved for the

90   use in combination with conjugated equine estrogens for hormone replacement therapy in

91   postmenopausal women (DUAVEE, Pfizer) in the US and for the prevention of osteoporosis as a

92   single agent in Europe [9, 15]. Importantly, it displayed strong antagonist and SERD profiles in

93   the breast while retaining beneficial agonist properties in the bone and did not stimulate

94   endometrial tissue in pre-clinical studies [9, 16, 17]. Further, BZA showed good oral

95   bioavailability and improved pharmacokinetics compared with fulvestrant (FULV) [9, 18].

96   In this study, breast cancer reporter gene assays reveal the inhibitory capacity of BZA against

97   the ERα mutants compared to the SERM 4-hydroxytamoxifen (4-OHT) and SERD FULV in

98   several ER+ breast cancer cell lines (MCF-7, ZR75, T47D). We further assessed the ability of

99   BZA to induce the degradation of WT, Y537S, and D538G somatic mutant ERα in MCF7 cells.

100   Additionally, because inhibitors of CDK4/6 combined with antiestrogens are approved for first

101   line therapy and beyond in metastatic ER+ breast cancers [19-21], we examined whether the

102   CDK4/6 inhibitor, palbociclib, can be used in combination with BZA to enhance the inhibition of

103   breast cancer cell proliferation. Importantly, comprehensive structural and biophysical studies

104   provide additional molecular insights into the chemical differences between BZA, 4-OHT, and

105   raloxifene (RAL, another SERM) that appear to underlie the SERD properties of BZA and its

106   improved inhibitory efficacy against the Y537S and D538G mutants in breast cancer cells. **Table**

107   **1** shows the chemical structures of the molecules examined in this study and summarizes their

108   clinical indications.

109   **Table 1:** Competitive inhibitors of estrogen receptor alpha.

| Antiestrogen	Class	Approved Clinical Indications
4-Hydroxytamoxifen (4-OHT)	SERM	• Adjuvant treatment for ER+ breast cancers [22]. • Metastatic Breast Cancer [23]. • Ductal Carcinoma in Situ [24]. • Reduction in Breast Cancer Incidence in High Risk Women [25].
Raloxifene (RAL)	SERM	• Osteoporosis in postmenopausal women [26]. • Reduction in Breast Cancer Incidence in High Risk Women[27].
Fulvestrant (FULV)	SERD	• First-line therapy for metastatic breast cancer [28]. • Postmenopausal women with progressive breast cancer following other antiestrogen therapy [29, 30].
Bazedoxifene (BZA)	SERM/SERD	• In combination with conjugated equine estrogens (DUAVEE) to prevent postmenopausal osteoporosis [15].

110

Results

Bazedoxifene Displays SERD Activity in MCF-7 Cells that Express WT ERα

113   To assess the ability of BZA to inhibit WT ERα in breast cancer cells, we examined its

114   impact on ERα transcriptional activity, degradation and cell growth in MCF-7 cells. 4-

115   hydroxytamoxifen (4-OHT) was used as a representative SERM and FULV was used as a

116   representative SERD (**Figure 1**). In MCF7 cells that expressed an ERE-luciferase reporter gene,

117   BZA was a more potent inhibitor of WT ERα transcription than either 4-OHT or FULV

118   (inhibition of luciferase IC_{50} for BZA = 0.12 nM, 4-OHT = 0.39 nM and FULV = 0.76 nM)

119   (**Figure 1A**). To test the effect of BZA on endogenous WT ERα transcriptional activity, qPCR

120   was used to quantify the relative mRNA levels of known ER target genes, including cyclin D1,

121   c-myc, CA12, and GREB1, in MCF-7 cells treated with estradiol (E2) or with E2 in combination

122   with BZA, 4-OHT or FULV at 10^{-8} and 10^{-6} M (antagonistic mode). For cyclin D1, 4-OHT

123   increased the mRNA level at 10^{-8} M and showed little effect at 10^{-6}M, while both FULV and

124   BZA decreased mRNA levels at 10^{-6} M (**Figure 1B**). The agonist activity of tamoxifen at low

125   concentrations has been described previously [31]. BZA increased c-myc mRNA levels at 10^{-8} M

126   while it significantly decreased c-myc mRNA at 10^{-6} M (**Figure 1C**). Presumably this effect is

127   similar to the behavior of low-level tamoxifen stimulation and merits further examination.

128   Interestingly, 10^{-6} M BZA showed the greatest reduction in mRNA levels of both CA12 and

129   GREB compared to 4-OHT and FULV (**Figure 1, D and E**).

130   As BZA was shown to behave as a SERM/SERD in previous studies [9, 17], we next

131   tested the activity of BZA as an inducer of ERα degradation and observed dose-dependent ER

132   degradation in MCF7 cells. Overall, BZA mediated similar levels of ERα degradation compared

133   to FULV (**Figure 1F**). In terms of cell growth inhibition, BZA showed an improved IC_{50}

134   compared to 4-OHT and in the same range as fulvestrant (BZA $IC_{50} = 2.4 \times 10^{-10}$ M, FULV $IC_{50} =$

135   3.1×10^{-10} M and 4-OHT $IC_{50} = 1.19 \times 10^{-9}$ M (**Figure 1G**). Together, these data indicate that BZA

136   degrades WT ERα in breast cancer cells and is more effective at inhibiting ER transcription and

137   cell growth than 4-OHT and FULV.

138
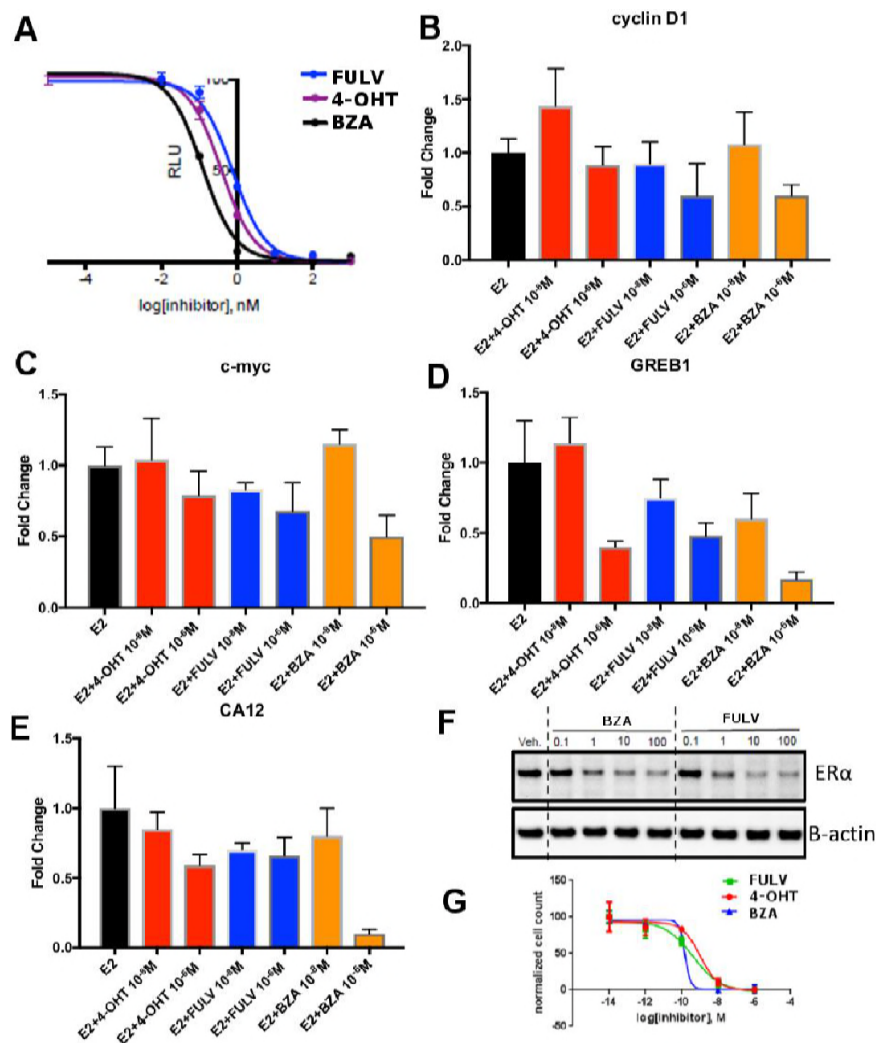
Figure 1: The inhibitory potency of BZA in MCF-7 cells. **A)** ERα transcriptional reporter gene assay in
cells treated with BZA, FULV, and 4-OHT. **B)** Relative cyclin D1 mRNA levels of in MCF-7 cells
treated with E2 plus 4-OHT, FULV, or BZA vehicle and normalized to E2. **C)** Relative c-myc mRNA
levelsMCF-7 cells treated with E2 plus 4-OHT, FULV, or BZA vehicle and normalized to E2. **D)**

143   Relative GREB1 mRNA levels in MCF-7 cells treated with E2 plus 4-OHT, FULV, or BZA vehicle and

144   normalized to E2. **E)** Relative CA12 mRNA levels of MCF-7 cells treated with E2 plus 4-OHT, FULV,

145   or BZA vehicle and normalized to E2. **F)** ERα degradation in MCF-7 cells with increasing doses of BZA

146   or FULV normalized to β-actin. **G)** Inhibition of cell growth with increasing concentrations of BZA,

147   FULV, or 4-OHT.

148   **BZA is a Potent Inhibitor of Activating Somatic Mutants of ERα in Breast Cancer Cells**

149   We next tested the activity of BZA in MCF7 cells that ectopically expressed theY537S

150   mutant ERα to determine the inhibition of Y537S mutant cell growth. BZA demonstrated an

151   increased potency compared to FULV and 4-OHT, with an IC_{50} of 1×10^{-10} M vs 2×10^{-9} M and

152   7×10^{-9} M, respectively (**Figure 2A**). In addition, qPCR data showed that BZA inhibited the

153   transcription of ERα target genes cyclin D1, c-Myc, and PR, in cells expressing the Y537S

154   mutant, in a dose-dependent manner, confirming the on-target effects of BZA in the presence of

155   the mutation (**Figure 2B**).

156   To evaluate the ability of BZA to induce WT and mutant ERα degradation in breast

157   cancer cells, we treated MCF-7 cells that ectopically expressed HA-tagged WT, Y537S and

158   D538G ERα with BZA and other ligands for comparison. Levels of WT and mutant ERα were

159   quantified using immunoblots with an anti-HA antibody. Cells were treated with 10 nM E2, or

160   100 nM 4-OHT, 100 nM BZA, 100 nM RAL, 1 μM FULV or vehicle for 24 hours before

161   immunostaining; 1 μM FULV was chosen because it was the minimal concentration necessary to

162   achieve maximal ERα degradation. All data were normalized to vehicle-treated cells. In cells

163   expressing HA-WT ERα, BZA and FULV induced degradation of the receptor to similar levels

164   while the amount of the receptor increased upon 4-OHT treatment and was slightly reduced with

165   E2 and RAL (**Figure 2C and D**). Interestingly, for the Y537S mutant, ERα expression remained

166   unchanged for E2 and FULV, while it increased for 4-OHT and RAL. Y537S ERα also

167   increased with BZA but less so than RAL or 4-OHT. Surprisingly, BZA degraded the D538G

168   ERα mutant to a greater extent than FULV while 4-OHT and RAL both increased its expression

169   after 24 hours. It should be noted that BZA and FULV elicited consistent WT and mutant ERα

170   degradation across all replicates (**Supplemental Figure 1**). However, 4-OHT and RAL elicited

171   slight variations in the actin-normalized quantity of ERα after 24-hours. Overall, these data

172   suggest that BZA degrades WT and D538G ERα in MCF7 cells, but that the Y537S mutant is

173   resistant to degradation. However, the levels of Y537S ERα in the BZA treated cells were still

174   reduced compared to 4-OHT and RAL treatment, consistent with the reduced activities

175   demonstrated by these compounds in MCF-7 reporter gene assays [2].
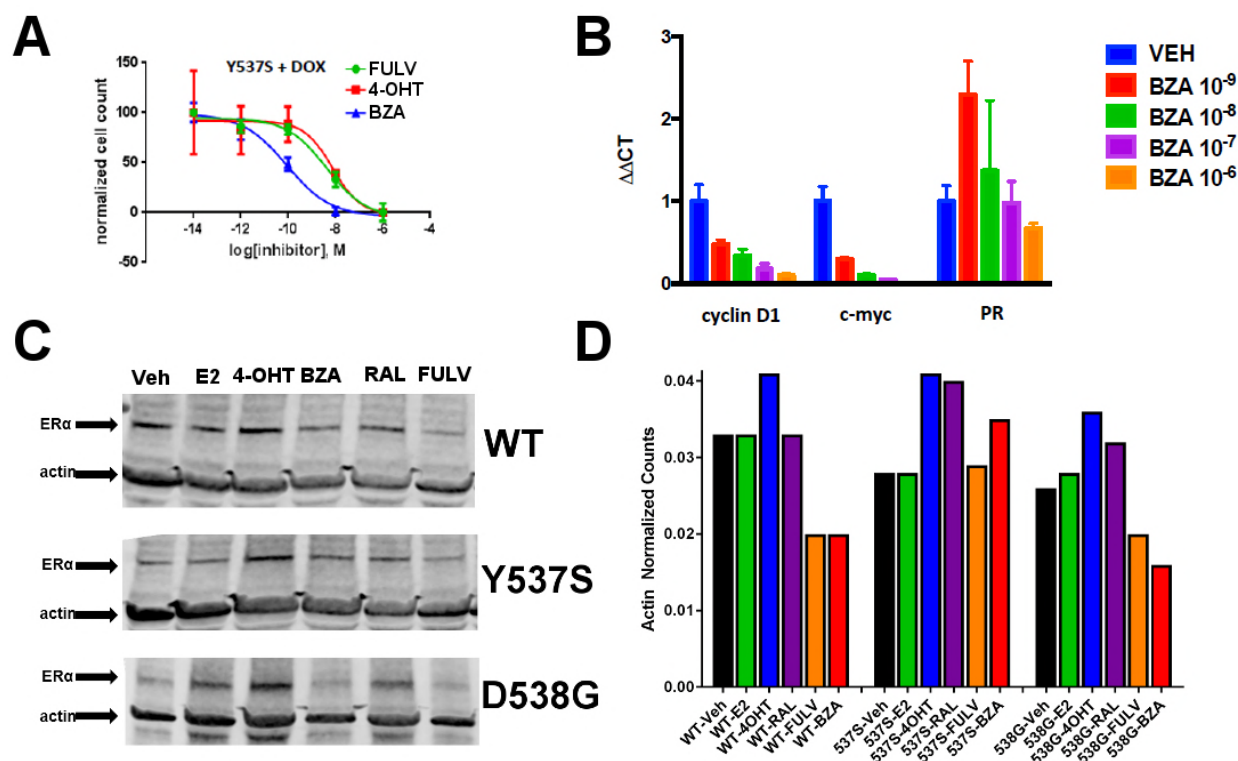
176
177   **Figure 2:** The ability of BZA to disrupt Y537S and D538G ERα activity. **A)** Cell growth in MCF-7 cells
178   with DOX-induced Y537S ERα expression. **B)** Inhibition of ERα target genes in DOX-induced Y537S
179   ERα expressed MCF-7 cells with increasing doses of BZA. **C)** Representative immunoblot of HA-ERα
180   WT, 537S, or D538G treated with E2, 4-OHT, BZA, RAL, or FULV for 24 hours. **D)** Representative
181   counts of HA-ERα from the immunoblot normalized to actin.

182

183   **Dual Treatment with BZA and Palbociclib**

184   CDK4/6 inhibitors have emerged as potent agents in the treatment of metastatic ER+

185   breast cancer in combination with endocrine treatment. Combined endocrine treatment with a

186   CDK4/6 inhibitor is now the standard of care in either first or second line treatment of metastatic

187   ER+ breast cancer [19-21]. Because BZA showed increased activity over FULV and 4-OHT, we

188   explored whether the activity of BZA combined with the CDK4/6 inhibitor, palbociclib (PB), in

189   multiple ER positive cell lines (MCF-7, ZR75, T47D) and long-term, estrogen-deprived (LTED)

190   ER+ MCF7 cells that mimic resistance to aromatase inhibitors. For the first three cell lines, the

191   combination of BZA and PB demonstrated the greatest arrest in cellular proliferation, whereas

192   for the LTED cells it was comparable to PB+FULV **(Figure 3A-D)**. Additionally, reduced

193   proliferation of MCF-7 cells expressing the Y537S mutant was observed for the BZA+PB

194   treatment compared to all other treatments (**Figure 3E and F**). Transcriptional reporter gene

195   assays in MCF7 cells showed that: 1. BZA had superior activity in the inhibition of ER

196   transcriptional activity compared to fulvestrant. In addition, palbociclib does not affect ER

197   transcriptional activity either as a single agent or in combination with BZA (**Figure 3G and 3H)**

198   . Similarly, immunoblotting for ER showed that treatment with PB does not affect BZA or

199   FULV induced degradation of ERα (**Figure 3I**). In sum, these data show that dual inhibition of

200   CDK4/6 with PB and ERα with BZA is an effective combination with significant activity against

201   breast cancer cells expressing WT or constitutively active mutant ERα.

202
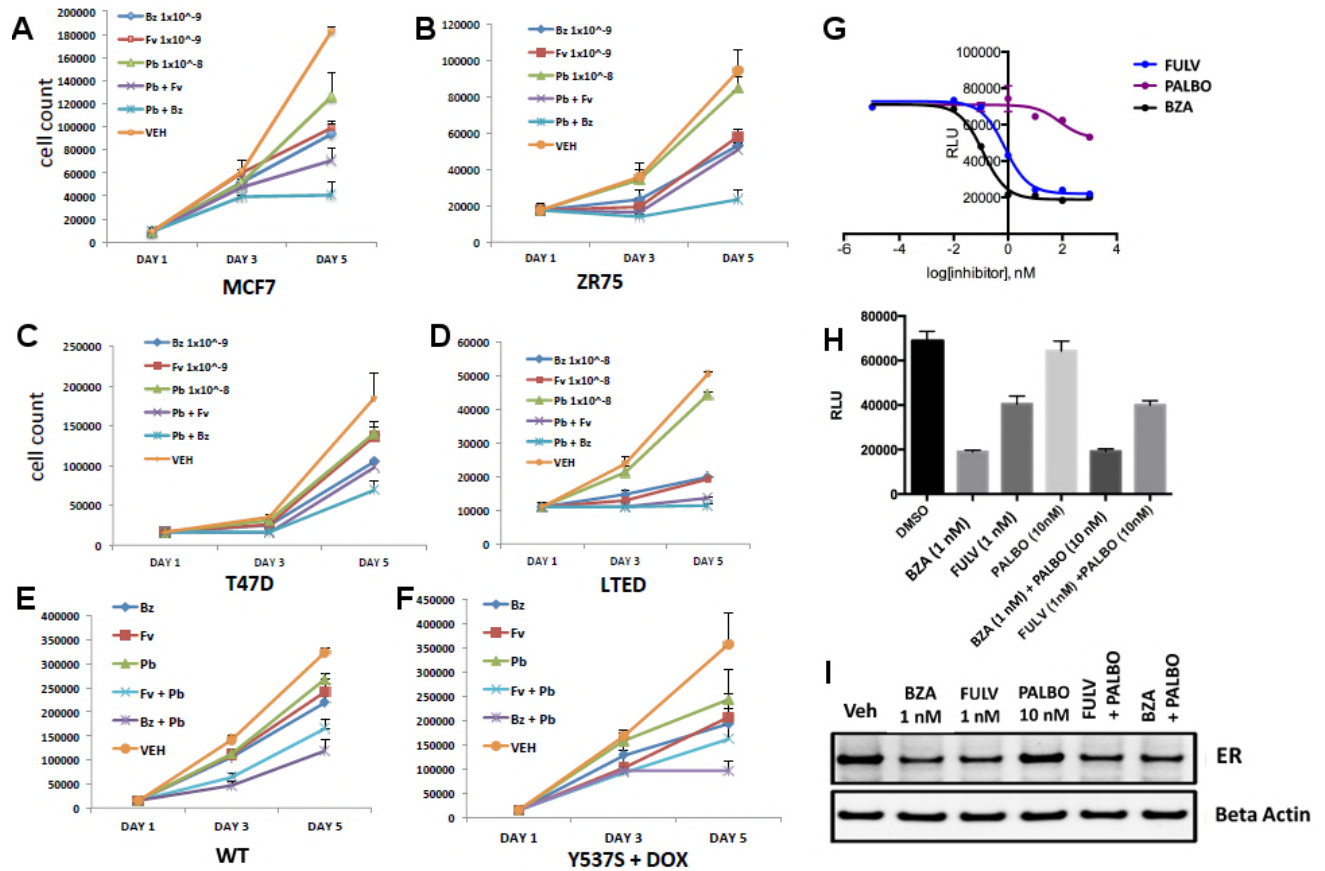
Figure 3: Combination treatment with CDK4/6 inhibitor and BZA. **A)** Cell growth inhibit with MCF7 breast cancer cells. **B)** ZR75 breast cancer cells. **C)** T47D breast cancer cells. **D)** LTED breast cancer cells. **E)** Non-induced MCF7 breast cancer cells with a dox-inducible ERα Y537S mutant. **F)** MCF7 cells expressing ERα Y537S. **G)** Dose-response curves for inhibition of ERα transcriptional activity in the presence of BZA, PALBO, and FULV in MCF7 cells. **H)** ERα transcriptional reporter gene assays for combination treatments. **I)** ERα stability resulting from combination treatments.

209

Coregulator Binding Specificity and Affinities of WT and Mutant ERα with BZA, 4-OHT, and FULV

Because hormone regulated coactivator recruitment is crucial for ERα genomic action and inhibition of coactivator recruitment is a key aspect of SERM-mediated ERα antagonism [32], we tested the effects of 4-OHT, BZA and FULV on co-regulator binding. We applied the Microarray Assay for Real-time Coregulator-Nuclear receptor Interaction (MARCoNI), which

216   allows the quantification of binding affinity of a nuclear receptor with co-regulator peptides. To

217   determine the effect of 4-OHT, BZA and FULV on co-regulator binding to WT, Y537S and

218   D538G ERα, MCF7 cells that ectopically express HA-tagged WT, Y537S, or D538G ERα were

219   used in conjunction with an HA antibody to detect ER binding to the co-regulator array.

220   Experiments were performed under E2 stimulated conditions for WT ER and under apo

221   conditions for mutant ERα. Overall, dose-dependent inhibition of co-regulator binding was

222   observed for the majority of co-regulator peptides with the three drugs (**Supplemental Figure**

223   **2A**). A comparison of EC_{50} levels for inhibition of co-regulator binding of the three ER

224   antagonists showed that EC_{50} levels for FULV in both the WT and mutant cells was higher, as

225   expected given the mechanism of action of FULV, compared to SERMs. The 4-OHT and BZA

226   EC_{50}s were higher in the presence of the Y537S and D538G mutations. Collectively, these

227   results show that differences in antagonistic activity manifested by the three endocrine treatments

228   are reflected by changes in co-regulator binding. There are significant differences among these

229   drugs in their antagonistic activity on WT-ER and mutant ER.

230   **SERMs and SERDs Abolish Hormone-Independent ERα-Coactivator Binding *In Vitro* and**

231   **Reverse Hormone Recruitment of Coactivators**

232   To further dissect the molecular basis for the reduced BZA, 4-OHT, and RAL

233   potency/efficacy observed with mutant ERs, biochemical coactivator recruitment and

234   competitive ligand-binding experiments were performed. As described previously [8], Förster

235   resonance energy transfer (FRET) assays were used to evaluate the interaction of wild type and

236   Y537S and D538G mutant ERα with steroid receptor coactivator 3 (SRC3), a key coregulator in

237   breast cancer cells. The nuclear receptor recognition domain (NRD) of SRC3 and LBD of the

238   ERs, were used in these experiments.

239   Previously, we showed that in the absence of hormone, SRC3 did not bind to WT ERα

240   LBD, whereas Y537S ERα bound SRC3 markedly in the absence of E2 with a 10-fold reduced

241   affinity, and D538G ERα bound SRC3 with a 100-fold reduced affinity compared to hormone

242   bound WT receptor [8]. To better ascertain the potency of ligands to inhibit coactivator

243   recruitment, we titrated the ligands into fixed concentrations of LBD and SRC3 and monitored

244   LBD-SRC3 interaction by a FRET assay; the three samples were primed with E2 to get a

245   measurable signal from WT and D538G ER. 4-OHT, BZA and RAL reversed the binding of

246   SRC3 NRD to the two mutant ERs and WT-ERα with similar potencies (**Supplemental Figure**

247   **2B**). Together, these data show that BZA, 4-OHT, and RAL inhibit both the basal and E2-

248   stimulated recruitment of SRC3 coregulator by the WT and mutant ERα *in vitro*.

249   **BZA, RAL and FULV Elicit Similar Reduced Binding Affinities for Y537S and D538G**

250   **Compared to WT ERα LBD**

251   To examine what role alterations in binding affinity may play in this reduced potency,

252   competitive [^{3}H]-E2 ligand binding assays ligand-binding experiments were used to examine the

253   effect of Y537S and D538G mutations on BZA, RAL, and FULV ER binding affinities *in vitro*.

254   We previously showed that the E2 and 4-OHT binding was significantly reduced for both the

255   Y537S and D538G mutants [8]. Affinities were reported using K_i values calculated from IC_{50}

256   values using the Cheng-Prusoff equation (**Supplemental Table 2**) [33]. The affinities of RAL,

257   BZA and FULV for the ERα mutants were reduced 9 to 27-fold relative to WT-ERα. It should be

258   noted that the binding affinity of 4-OHT remained the highest compared to RAL, BZA and

259   FULV against the mutant LBDs. The binding affinities of all tested antiestrogens were somewhat

260   more reduced in D538G than in Y537S. However, FULV and BZA demonstrated the highest

261   potencies in the transcriptional reporter gene assays, even though they exhibited reduced

262   affinities compared to 4-OHT. Therefore, our data indicate that other factors beyond the reduced

263   binding affinity of mutant LBDs for SERM or SERD must play a role in their decreased potency.

The SERD Properties of BZA Arise from its Disruption of Helix 12

265   X-ray crystallography was used to reveal the structural details of BZA's antiestrogen

266   properties. An x-ray crystal structure for the WT ERα LBD, in complex with BZA was solved to

267   2.4 Å with two dimers in the asymmetric unit (ASU) (PDB: 4XI3). The BZA ligand and H12 are

268   well resolved in each monomer in the ASU; poorly resolved residues were not included in the

269   model. **Supplemental Figure 3** shows the observed difference map density for the BZA ligand

270   for chain A. We were unable to obtain diffraction quality crystals with BZA or RAL in complex

271   with either the Y537S or D538G mutant LBDs.

272   Clear structural differences are apparent compared to the previously published molecular

273   modeling and docking simulations of the ERα LBD-BZA complex [34]. Specifically, the C3

274   methyl on the indole ring of BZA appears to shift the core of the molecule away from M386,

275   L391 and L428 and towards H12. BZA is most structurally similar to RAL; however, BZA

276   displays more SERD-like behavior [9]. **Figure 4** shows a superposition of the ERα LBD-BZA or

277   RAL x-ray crystal structures. Interestingly, the distal phenol on BZA appears to form a hydrogen

278   bond with improved binding geometry to H524 compared to the distal phenol of RAL. This

279   suggests that the ketone on the RAL linker constrains the phenyl group, sterically precluding the

280   adoption of an ideal hydrogen bonding geometry with H524. The core differences for BZA

281   broadcast down the linker arm to alter its vector towards H12 where the azepan ring now pushes

282   against V534 and P535 (**Figure 4B**). The alterations to V534 and P535 propagate to H12 which

283   appears displaced out of the AF-2 cleft into a less stable orientation.

284
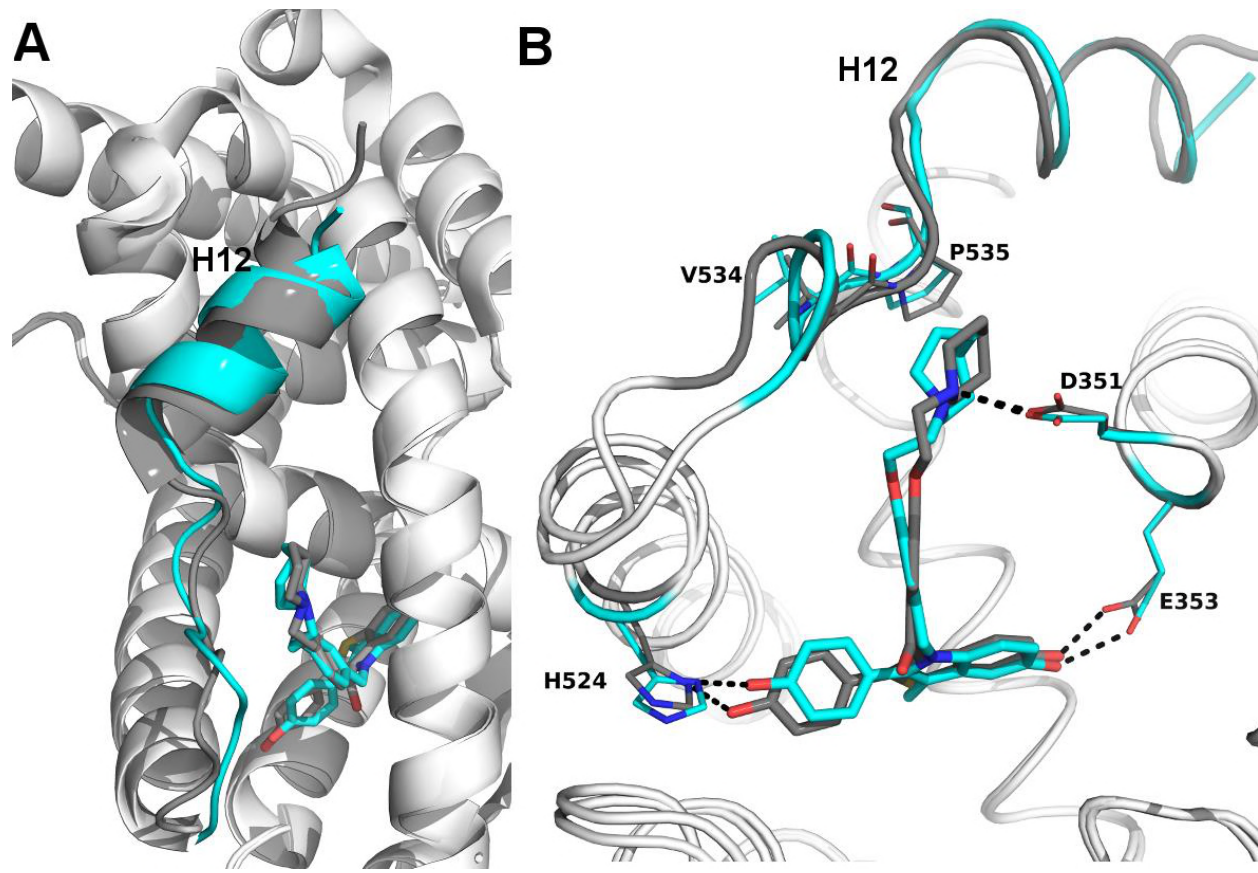
Figure 4: Structural Basis for the SERD properties exhibited by BZA. A) Overlay of BZA (cyan) with RAL (grey) x-ray crystal structures showing differences in H11-12 loop and H12 orientation. B) Hydrogen bonds (dashed lines) formed by BZA and RAL in the binding pocket and highlighting differences in H11-12 loop and H12 conformation. PDBs: 1ERR and 4XI3.

289

BZA Binding Conformation is Energetically Favored Compared to RAL

291   Quantum mechanical calculations were employed to determine whether inherent

292   differences in the BZA and RAL ligands accounted for differences in antagonist potency. A

293   significant energetic shift was observed over the time-course of the scans, revealing that the BZA

294   arm can adopt a set of torsion angles with significantly reduced energetic penalties compared to

295   RAL (**Figure 5A**). Importantly, the energetic minima well is significantly broader for BZA

296   compared to RAL, indicating that the angles adopted by BZA in the ERα ligand-binding site are

297   more favorable than RAL. Furthermore, an energetic penalty of approximately 1 kcal/mol would

298   be incurred by RAL to adopt the same conformation observed for BZA in the x-ray crystal

299   structure. Together these data show that the BZA ligand itself possesses physical properties that

300   are more favorable to impact ERα H12 compared to RAL.

BZA and FULV Reduce the Impact of Y537S and D538G Mutations on Helix 12 Dynamics

302   SERDs competitively bind to the ERα LBD and destabilize helix 12 (H12), leading to

303   proteosomal degradation, while SERMs push the helix into the AF2 cleft to block coregulator

304   binding [8]. Furthermore, AZD9496, a newer orally available SERD pushes H12 into the AF2

305   cleft but destabilizes the helix [13]. Previous work showed that the Y537S and D538G mutants,

306   in complex with 4-OHT, adopts an altered antagonist conformation with respect to the WT-4-

307   OHT complex [8]. Here, we explored how Y537S and D538G ERα LBD mutations impact H12

308   mobility in the BZA complex using differential hydrogen-deuterium exchange mass

309   spectrometry (HDX-MS). For comparisons we chose E2 as a representative hormone, FULV as a

310   representative SERD, and 4-OHT as a representative SERM. Average time-dependent amide-

311   deuterium uptake kinetics is indicative of conformational flexibility in proteins with highly

312   dynamic regions being more susceptible to solvent deuterium exchange compared to

313   conformationally rigid regions. As expected, addition of E2 resulted in an increased protection

314   against exchange in H12 (inferred as increased stability or less dynamic), and this protection was

315   enhanced for the Y537S and D538G mutants (**Supplemental Figure 4**). Also, FULV treatment

316   led to increased D_2O uptake in H12 (interpreted as destabilization) of regions near H12 in both

317   the WT and D538G mutant (**Supplemental Figure 5**), consistent with its SERD-like properties.

318   Unfortunately, we were unable to collect HDX data for the Y537S mutant with FULV because it

319   precipitated out of solution. Similar to previously published data [8], binding of 4-OHT resulted

320   in decreased stability of H12 with the Y537S compared to D538G and WT receptor

321   (**Supplemental Figure 6**), suggesting that these mutants resist the ability of the SERM to alter

322   their structure. Interestingly, addition of BZA did not increase the stability (lesser protection) of

323   the region near H12 to as great of an extent as 4-OHT in WT and mutant ERα LBDs, suggesting

324   that BZA-bound ERα adopts a less stable antagonist conformation than 4-OHT-bound ERα

325   (**Supplemental Figure 7**), consistent with the crystal structure. These data suggest that, while

326   their antagonist conformations are altered by Y537S or D538G mutations, the ERα-BZA and

327   FULV complexes maintain potency because they resist the stabilizing impact of the mutations

328   better than 4-OHT.

329   **How Y537S and D538G ERα LBD Mutants Alter the BZA Antagonist Structure**

330   To understand the structural basis for the reduced BZA degradation of Y537S compared

331   to WT ERα, atom-level explicit-solvent molecular dynamics (MD) simulations for the LBD of

332   ERα Y537S-BZA and D538G-BZA were performed using the WT-BZA crystal structure as

333   template. When compared to the WT-4-OHT structure (PDB: 3ERT), the D538G-4-OHT

334   structure displayed a significantly altered H11-12 loop, which leads to a perturbed H12

335   antagonist state (**Figure 5B**) [8].

336   MD simulations show that H12 of both BZA-bound mutants remain close to an

337   antagonist conformation (**Figure 5B, D**). Furthermore, H12 conformational fluctuations

338   observed in MD simulations are less pronounced in Y537S-BZA than they are in D538G-BZA

339   (**Figure 5C**), which echoes the aforementioned reduced H12 dynamics observed in HDX-MS

340   data and agrees with our result that Y537S reduces BZA activity more than D538G does. Over

341   the course of the simulations, the Y537S-BZA structure shows a hydrogen bond formation

342   between E380 and S537 (**Figure 5B**), which could contribute to fewer H12 conformational

343   fluctuations in Y537S ERα. It should be noted that this hydrogen bond is not sterically allowed

344   in the WT-BZA crystal structure. This predicted hydrogen bond may stabilize H12 in the AF-2

345   cleft relative to WT. The simulated H11-12 loop conformations for both Y537S-BZA and

346   D538G-BZA resemble WT-BZA or D538G-4-OHT, being closer to the ligand binding site, than

347   they do to WT-4-OHT. The D538G mutation further increases the conformational variance of

348   the H11-12 loop compared to Y537S (**Figure 5C**), which can be explained by the lack of a

349   hydrogen bond in Y537S and the greater backbone conformational freedom allowed by the

350   mutant glycine residue. Additionally, the H11-12 loop of both Y537S and D538G appears

351   further away from the protein core and BZA compared to that of WT (**Figure 5B, D**). We

352   hypothesize that the varied conformations and increased dynamics of the H11-12 loop in both

353   ERα mutants makes it more difficult for BZA to maintain sufficient interactions with the loop to

354   disrupt the ER antagonist conformation. Together, these data show that both mutations produce a

355   stable antagonist conformation, especially at H12, and reduce the SERD-like properties of BZA

356   by lessening its ability to disrupt the H11-12 loop and stabilize H12 in the AF-2 cleft.

357
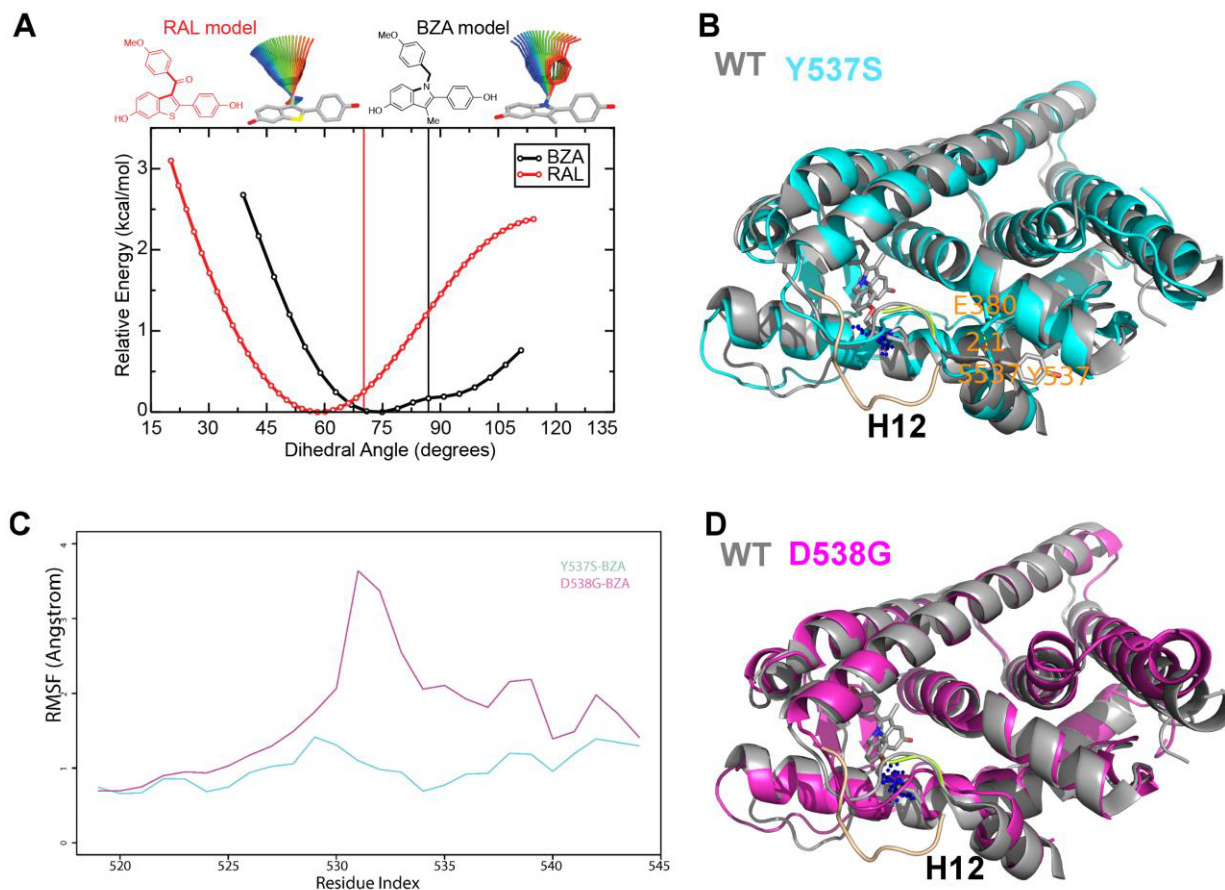
Figure 5: A) QM scan of RAL and BZA arm torsion angle energetics. **B)** Overlaid representative calculated structure of Y537S-BZA (cyan) closest to the last 50-ns average from molecular dynamics (MD) simulation and the WT-BZA structure, vertical lines represent the ligand binding conformation in the x-ray crystal structure. Nitrogen atoms of the azepane part of BZA for the last 50-ns MD ensemble are shown in blue spheres near H12. Loop H11-12 is also shown for crystal structures of WT-4-OHT (wheat; PDB: 3ERT) and D538G-4-OHT (yellow; PDB: 4Q50). **C)** Root mean squared fluctuations of ERα LBD residues, including the C-end of H11 (resi. 519-527), the loop H11-12 (resi. 528-535), and H12 (resi. 536-544), in the last 50-ns MD simulations for Y537S-BZA (cyan) and D538G-BZA (magenta). **D)** Overlay of a representative structure of D538G-BZA (magenta) from MD simulations and the same WT-BZA structure (gray) as in **B)**.

369

370

Discussion

371

372   Somatic mutation to *ESR1* following prolonged estrogen-deprivation therapy represents a

373   newly appreciated mechanism of acquired hormone resistance in metastatic breast cancer. The

374   two most prevalent mutations,Y537S and D538G, give rise to a dysfunctional receptor that

375   escapes hormone regulation and has decreased sensitivity to inhibition by 4-OHT and fulvestrant

376   [8]. Newly characterized orally available pure antiestrogens (*e.g.,* GDC-0927, AZ9496, and

377   RAD1901) are emerging as potentially potent inhibitors of these mutants, but their long-term

378   clinical utility is unknown and their side effect profiles have not been studied in large patient

379   populations [12, 14]. Because BZA is already clinically approved for use in hormone

380   replacement therapy and is a potent ERα antagonist in the breast, an agonist in bone, and neutral

381   in the endometrium with long-term safety data in thousands of patients, we explored its ability to

382   inhibit the Y537S and D538G ERα somatic mutants in breast cancer [9].

383   We first quantified the ability of BZA to disrupt WT and mutant ERα transcription,

384   induce degradation, and inhibit cell growth in MCF-7 cells. These data show that BZA has

385   increased activity, compared to the SERD FULV and SERM 4-OHT, toward inhibition of cell

386   growth and ERα transcriptional activity. Further, BZA elicited degradation of WT receptor,

387   although not as much as FULV. Importantly, BZA reduced the levels of Y537S ERα relative to

388   RAL and 4-OHT. Together these data suggest that the ability of BZA to degrade ERα confers an

389   inhibitory advantage over 4-OHT in the context of the somatic mutants. Additionally, combined

390   treatment with BZA and the CDK4/6 inhibitor palbociclib resulted in additional inhibitory

391   potency of cellular proliferation in breast cancer cells expressing both WT and Y537S ERα

392   without impacting BZA's action. As such, combination BZA-CDK4/6 treatment shows

393   significant potential in cell line experiments and merits further evaluation.

394   Comprehensive structural-biochemical investigations were undertaken to understand the

395   basis for the SERD-like properties of BZA and its improved potency against the Y537S and

396   D538G ERα LBD mutants compared to 4-OHT. Biochemical coactivator studies using

397   recombinant ERα LBD demonstrated that BZA could inhibit the both basal and E2-induced

398   recruitment of coregulators *in vitro*, while ligand-binding assays showed that the Y537S and

399   D538G mutants had significantly reduced affinities for BZA, 4-OHT, RAL, and FULV.

400   Interestingly, an HDX MS comparison of BZA, 4-OHT, and FULV suggested that FULV and

401   BZA can both resist the impact of somatic mutation on their antagonist binding conformations

402   compared to 4-OHT. An x-ray crystal structure of the WT-BZA complex revealed that

403   differences in the core of the molecule translated to an altered vector of the linker arm, resulting

404   in contacts with the H11-12 loop and a perturbed H12 antagonist binding mode. This less stable

405   H12 antagonist conformation likely explains the SERM/SERD properties of BZA, wherein it

406   allows H12 to adopt an antagonist conformation (like a SERM) that is somewhat destabilized,

407   although not as destabilized as when FULV is bound.

408   Atomistic MD simulations were used to examine the molecular basis for the observed

409   decrease in degradation of ERα within breast cancer cells expressing the Y537S and D538G

410   mutants. Both mutants stabilized the antagonist conformation of H12 in the AF-2 cleft, while the

411   Y537S appeared to be the more stable of the two by forming a hydrogen bond between S537 and

412   E380. Interestingly, E380Q has also been found to be a recurrent ESR1 mutation able to confer

413   endocrine resistance. MD simulations also suggest that these mutants have varied conformations

414   and increased dynamics of loop H11-12, which potentially reduces BZA's ability to disrupt ER

415   antagonist conformations. Together these results suggest that BZA retains its SERM antagonist

416   properties within breast cancer cells expressing Y537S and D538G mutant ERα to a greater

417   extent than 4-OHT but its SERD-like properties are diminished. The reduced potency on the

418   mutants likely derives from the stabilization of the apo receptor in the agonist conformation,

419   which reduces the on rate of ligand binding [8], reflecting that the agonist conformer blocks

420   ligand exchange [35].

421   Overall, our findings show the molecular basis for the SERD-like activity of BZA and its

422   potential advantage with and without CDK4/6 inhibitor, versus 4-OHT, to inhibit the Y537S and

423   D538G ERα mutants. Importantly, interrogating the structural details of BZA-ERα LBD binding

424   suggests that molecules with improved pharmacological profiles that specifically disrupt the

425   H11-12 loop at H12 will have clear advantages against breast cancer cells expressing WT,

426   Y537S, and D538G ERα. **Figure 6** summarizes how BZA achieves SERM/SERD activity

427   compared to SERM or agonist compounds. In fact, the newer SERM/SERDs and SERDs with

428   improved pharmacologic profiles (*e.g.,* AZ9496) appear to do so using a similar mechanism [13].

429   Therefore, further preclinical evaluation of BZA with and without a CDK4/6 inhibitor should be

430   conducted in context of breast cancer cells expressing the Y537S and D538G somatic mutant

431   ERα. In addition, the ability of other new SERDs to withstand the impact of Y537S and D538G

432   mutations on their antagonist binding modes should be investigated.
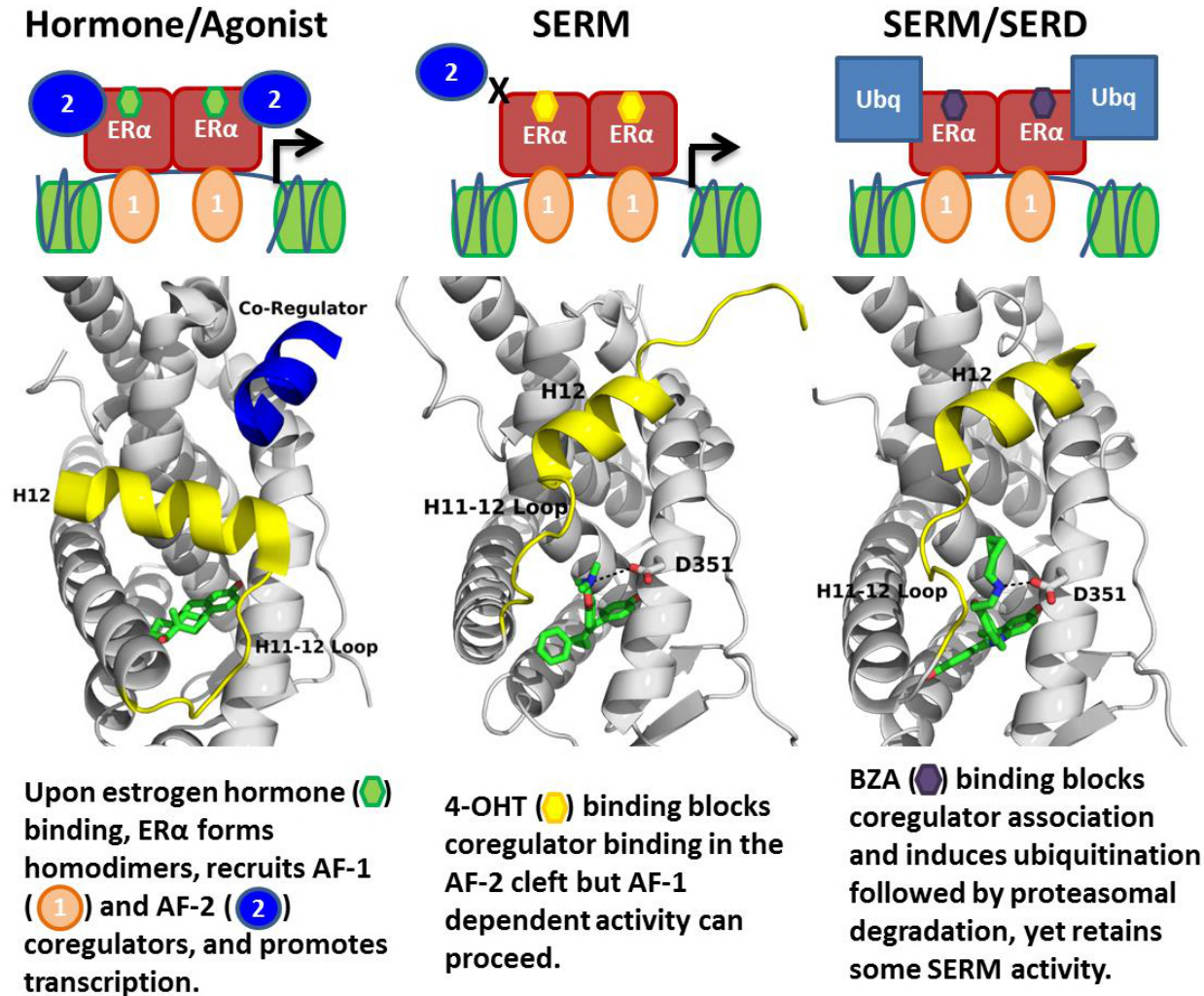
Figure 6: Summary of BZA's SERM/SERD activity compared to SERMs and agonist compounds.

433

434

435

436

437

438

439

440

Materials Methods

Breast Cancer Cellular Reporter Gene Assays

Luciferase reporter assay system (Promega) was used to monitor luciferase activity in MCF7 cells with stable expression of ERE luciferase per the manufacturer's recommendations, using a single tube luminometer (BD Monolight 2010). MCF7 cells were plated in 6-well plates and treated with increasing doses of BZA, FULV or 4-OHT (0 / 0.01 / 0.1 / 1 / 10 / 100 / 1000nM) in complete medium for 24 hours. All studies were performed in triplicates, and luciferase results are reported as relative light units (RLU) and normalized with β-Galactosidase activity using Mammalian β-gal assay kit (Thermo Scientific). Mycoplasma was tested every 6 weeks in these cells and no mycoplasma was detected in the MCF-7 cell lines using the MycoAlert Mycoplasma Detection Kit (Lonza). MCF-7 cells were purchased directly from ATCC and the studies were completed within 1 year of purchase. Cells reached a maximum of 30 passages during these studies.

ERα Stability Immunoblots

Tet-ON MCF7 cells lines (HA-ERα WT, HA-ERα Y537S, HA-ERα D538G) were cultured in DMEM supplemented with 10% fetal bovine serum (FBS), 2 mM L-glutamate, 1% penicillin-streptomycin, 100 μg/mL geniticin, and 100 μg/mL hygromycin. Before western blotting experiments, 300,000 cells were plated in each well of a 6-well culture dish and cultured for 48 hours in DMEM supplemented with 10% charcoal-stripped FBS (SFBS), 2 mM L-glutamate, 1% penicillin-streptomycin, and 0.2 μg/mL doxycycline. Compounds were diluted in ethanol or DMSO. Cells were treated with either 10 nM estradiol (Sigma), 1 μM FULV (Tocris), 100 nM Ral (Sigma), 100 nM BZA (Pfizer), 100 nM 4-OHT (Tocris), or vehicle (ethanol) for 24 hours.

463   Subsequently, cells were washed twice with 1 mL of ice-cold PBS, harvested via scraping, and

464   pelleted at 4 ^{o}C. Cells were resuspended in 50 μL lysis buffer [0.1% CHAPS, 50 mM HEPES

465   (pH 8.0), 120 mM NaCl,1mM EDTA, 10 mM Na pyrophosphate, and 10 mM glycerophosphate;

466   supplemented with a protease inhibitor cocktail solution III (CalBiochem)]. Cells were lysed via

467   3 freeze-thaw cycles. Lysates were then pelleted at 4 ^{o}C, and 100 μg of protein was mixed with

468   standard 2x Laemmli buffer. Samples were loaded onto a 10% SDS-polyacrylamide

469   electrophoresis gel, transferred after electrophoresis onto nitrocellulose membrane, and

470   immunoblotted using anti-HA-tag (Cell Signaling C29F4) and anti-actin (Santa Cruz

471   Biotechnology AC-15) antibodies. Membranes were probed using anti-rabbit 800 nm

472   (Rockland) and anti-mouse 680 nm (Rockland) and imaged on the Licor Odyssey. Membrane

473   intensities were normalized to actin control and quantified using ImageStudio. Mycoplasma was

474   tested every 6 weeks in these cells and no mycoplasma was detected in any of the Tet-ON MCF-

475   7 cell lines using the MycoAlert Mycoplasma Detection Kit (Lonza).

476

477   **Co-Regulator Interaction Profiling**

478   This method has been described previously [36]. Cell lysates of MCF7 cells expressing HA-

479   tagged WT-ER, Y537S mutant ER and D538G mutant ER were quantified by ELISA (Active

480   Motif, USA) to enable equimolar input. An array with a set of immobilized peptides representing

481   coregulator-derived NR-binding motifs was incubated with a reaction mixture of crude lysate,

482   vehicle (2% DMSO) with or without 1 μM 17β-estradiol (E2), increasing concentrations of BZA,

483   4-OHT or FULV (0.1, 1, 10, 100, 1000 nM) and anti-HIS-Alexa488 (Qiagen, USA). Incubation

484   was performed for 40 minutes at 20 °C, followed by removal of unbound receptor by washing

485   and generation of a TIFF image of each array using a PamStation96 (PamGene International).

486   Image processing and quantification of ERα binding to each peptide on the array was performed

487   by Bionavigator software (PamGene International).

488   **Coactivator Binding Assays**

489   *Protein preparation for TR-FRET*. Expression, purification, and site-specific labeling of the

490   ERα-LBD was performed as described previously [37]. Generation of the nuclear receptor

491   interaction domain (NRD) of human SRC3 coactivator has also been described previously [38].

492   ERα LBD and the SRC3 fragment were labeled with Mal-dPEG4-biotin (Quanta BioDesign,

493   Powell, OH), and 5-iodoacetamido fluorescein (Molecular Probes, Invitrogen, Eugene, OR),

494   respectively.

495   *Coactivator Recruitment with Ligand Titration.* To raise the background level of SRC3 NRD

496   binding, the ERα LBD preparation (1 nM ER-LBD, 0.25 nM SaTb, 100 nM SRC3-fluorescein)

497   was primed with 20 nM E2, and then increasing ligand concentrations (from 3×10^{-12} to 3×10^{-7}

498   M) were added. Diffusion-enhanced FRET was determined by a parallel incubation without

499   biotinylated ER-LBD and subtracted as a background signal. The time-resolved Förster

500   resonance energy transfer measurements were performed with a Victor X5 plate reader (Perkin

501   Elmer, Shelton, CT) with an excitation filter at 340/10 nm and emission filters for terbium and

502   fluorescein at 495/20 and 520/25 nm, respectively, with a 100-μs delay [39-41]. The data,

503   representing 2–3 replicate experiments, each with duplicate points, was analyzed using

504   GraphPad Prism 4, and are expressed as the IC_{50} in nM.

505   **Ligand Binding Assays**

506   The dissociation constant, (K_d) of estradiol binding to each ER was measured by saturation

507   binding with [^{3}H]17β-E_2 and Scatchard plot analysis [42], as described previously [8, 43].

508   Relative binding affinities (RBA) were determined by a competitive radiometric ligand binding

509   assay with 2 nM [^{3}H]E2 as tracer [8]. Incubations were at 0 °C for 18–24 hr. Hydroxyapatite was

510   used to adsorb the receptor-ligand complex, and unbound ligand was washed away. The

511   determination of the RBA values is reproducible in independent experiments with a CV of 0.3,

512   and the values shown represent the average ± range or SD of two or more separate

513   determinations. K_i was determined by the Cheng-Prusoff equation [33] $K_i = IC_{50}/(1 + [tracer$

514   total$/K_d$ of tracer]).

515   **Hydrogen/Deuterium Exchange-Mass Spectrometry (HDX-MS)**

516   Solution-phase amide HDX experiments were carried out with a fully automated system (CTC

517   HTS PAL, LEAP Technologies, Carrboro, NC; housed inside a 4°C cabinet) as described

518   previously [8] with slight modifications.

519   *Peptide Identification.* Peptides were identified using tandem MS (MS^2 or MS/MS) experiments

520   performed with a LTQ linear ion trap mass spectrometer (LTQ Orbitrap XL with ETD,

521   ThermoFisher, San Jose, CA) over a 70 min gradient. Product ion spectra were acquired in a

522   data-dependent mode and the five most abundant ions were selected for the product ion analysis

523   per scan event. The MS/MS *.raw data files were converted to *.mgf files and then submitted to

524   MASCOT ver2.3 (Matrix Science, London, UK) for peptide identification. The maximum

525   number of missed cleavage was set at 4 with the mass tolerance for precursor ions +/- 0.6 Da and

526   for fragment ions +/- 8ppm. Oxidation to Methionine was selected for variable modification.

527   Pepsin was used for digestion and no specific enzyme was selected in the MASCOT during the

528   search. Peptides included in the peptide set used for HDX detection had a MASCOT score of 20

529   or greater. The MS/MS MASCOT search was also performed against a decoy (reverse) sequence

530   and false positives were ruled out. The MS/MS spectra of all the peptide ions from the MASCOT

531   search were further manually inspected and only the unique charged ions with the highest

532   MASCOT score were used in estimating the sequence coverage and included in HDX peptide

533   set.

534   *HDX-MS analysis.* For differential HDX experiments, 5 μL of a 10 μM ERα LBD (Apo or in

535   complex with 10-fold excess compound) was diluted to 25 μL with D_2O-containing HDX buffer

536   (20 mM Tris-HCl pH 8.0, 150 mM NaCl, 5% glycerol, 1 mM DTT) and incubated at 4 °C for 10

537   s, 30 s, 60 s, 900 s, and 3600 s. Following on-exchange, unwanted forward or backward

538   exchange is minimized, and the protein is denatured by dilution to 50 μL with 0.1% TFA in 5 M

539   urea with 50mM TCEP (held at 4 °C, pH 2.5). Samples are then passed across an immobilized

540   pepsin column (prepared in house) at 50 μL min−1 (0.1% TFA,15 °C), and the resulting peptides

541   are trapped onto a C_8 trap cartridge (Thermo Fisher, Hypersil Gold). Peptides were then gradient

542   eluted (5% CH_3CN to 50% CH_3CN, 0.3% formic acid over 6 min, 4 °C) across a 1mm × 50 mm

543   C_{18} analytical column (Hypersil Gold, Thermo Fisher) and electrosprayed directly into a high

544   resolution orbitrap mass spectrometer (LTQ Orbitrap XL with ETD, Thermo Fisher). Percent

545   deuterium exchange values for peptide isotopic envelopes at each time point were calculated and

546   processed using HDX Workbench [44]. Each HDX experiment was carried out in triplicate with

547   a single preparation of each protein-ligand complex. The intensity weighted mean m/z

548   centroid value of each peptide envelope was calculated and subsequently converted into a

549   percentage of deuterium incorporation. This is accomplished by determining the observed

550   averages of the undeuterated and using the conventional formula described elsewhere

551   [45]. Statistical significance for the differential HDX data is determined by an unpaired t-test for

552   each time point, a procedure that is integrated into the HDX Workbench software

553   [44]. Corrections for back-exchange were made on the basis of an estimated 70% deuterium

554   recovery and accounting for 80% final deuterium concentration in the sample (1:5 dilution in

555   D_2O HDX buffer).

X-ray Crystallographic Analysis of the WT ERα LBD-BZA Complex

557   The 6×His-TEV-tagged ERα-L372S, L536S double mutant LBD was expressed in *E.coli*

558   BL21(DE3) and purified as described [46]. LBD (10 mg/mL) and incubated with 1 mM BZA

559   overnight at 4 °C. LBD-BZA was crystallized using vapor diffusion by hanging drop in 33%

560   PEG 3,350, 100 mM Tris pH 6.6, and 250 mM $MgCl_2$. Diffraction data were collected at the

561   Canadian Light Source at beamline 08ID-1 at a wavelength of 0.97 Å. Indexing, scaling, and

562   structure refinement were performed as described [8]. **Supplemental Table 1** shows data

563   collection and refinement statistics. Final coordinates were deposited in the Protein Databank

564   with the accession code 4XI3.

Quantum Mechanical Calculations

566   Torsion scans were performed on the bond connecting the internal subsituents to the central core

567   for each ligand. The ligand coordinates were extracted from x-ray crystal structures of BZA

568   (PDB code 4XI3) and RAL (PDB code 2QXS) and all hydrogens were added. Relaxed potential

569   energy surface scans in which the remainder of the structure is geometry optimized at each

570   torsion step were prepared and analyzed using the torsion scan module of the Force Field Toolkit

571   [47] (ffTK) plugin of VMD [48]. Quantum mechanical calculations were performed using

572   Gaussion G09 [49] at the MP2 level of theory with a 6-31G* basis set. Both ligands were

573   scanned using a bidirection technique originating from the crystal structure conformation and

574   scanning outward in the (+) and (-) directions independently. The BZA ligand was scanned in 4-

575   degree increments while the RAL ligand required a smaller 2-degree step size to avoid

576   discontinuities due to broader conformational changes when taking larger steps.

577   **Molecular Dynamics Simulations**

578   *Ligand parameterization.* A 3D structure of BZA (without hydrogen atoms) was first built using

579   the computer program GaussView (version 4.1.2; part of the computer program Gaussian 03

580   [50]. The remaining ligand parameterization was carried out as described [8].

581   *Structure preparation, molecular dynamics, data visualization and analysis.* WT-BZA (PDB:

582   4XI3) was used as a template to construct starting structures of Y537S-BZA and D538G-BZA.

583   Specifically, chains A and C were chosen among the three dimers in 4XI3 for having the least

584   missing residues in the loop H11-12 region, with ions removed and water molecules retained.

585   Side chain atoms of mutation sites (residue 537 and 538, respectively) were also replaced with

586   the mutant residues. Otherwise, structures were prepared, molecular dynamics were calculated,

587   and data were analyzed/visualized as described [8].

588

589

590

591

592

593

594

Acknowledgements

References Cited

616

617 1.   Frasor, J., et al., *Selective Estrogen Receptor Modulators.* Cancer Research, 2004. **64**(4): p. 1522.

618 2.   Toy, W., et al., *ESR1 ligand-binding domain mutations in hormone-resistant breast cancer.* Nat
619   Genet, 2013. **45**(12): p. 1439-45.

620 3.   Shang, Y. and M. Brown, *Molecular Determinants for the Tissue Specificity of SERMs.* Science,
621   2002. **295**(5564): p. 2465.

622 4.   Jeselsohn, R., et al., *ESR1 mutations-a mechanism for acquired endocrine resistance in breast*
623   *cancer.* Nat Rev Clin Oncol, 2015. **12**(10): p. 573-83.

624 5.   Jeselsohn, R., et al., *Emergence of constitutively active estrogen receptor-alpha mutations in*
625   *pretreated advanced estrogen receptor-positive breast cancer.* Clin Cancer Res, 2014. **20**(7): p.
626   1757-67.

627 6.   Niu, J., et al., *Incidence and clinical significance of ESR1 mutations in heavily pretreated*
628   *metastatic breast cancer patients.* Onco Targets Ther, 2015. **8**: p. 3323-8.

629 7.   Nettles, K.W., et al., *NFkappaB selectivity of estrogen receptor ligands revealed by comparative*
630   *crystallographic analyses.* Nat Chem Biol, 2008. **4**(4): p. 241-7.

631 8.   Fanning, S.W., Mayne, C.G., Dharmarajan, V., Carlson, K.E., Martin, T.A., Novick, S.J., Toy, W.,
632   Green, B., Panchamukhi, S., Katzenellenbogen, B.S., Tajkhorshid, E., Griffin, P.R., Shen, Y.,
633   Chandarlapaty, S., Katzenellenbogen, J.A., Greene, G.L., *Estrogen Receptor Alpha Somatic*
634   *Mutations Y537S and D538G Confer Breast Cancer Endocrine Resistance by Stabilizing the*
635   *Activating Function-2 Binding Conformation.* eLife, 2016.

636 9.   Wardell, S.E., et al., *Bazedoxifene exhibits antiestrogenic activity in animal models of tamoxifen-*
637   *resistant breast cancer: implications for treatment of advanced disease.* Clin Cancer Res, 2013.
638   **19**(9): p. 2420-31.

639 10. Garner, F., et al., *RAD1901: a novel, orally bioavailable selective estrogen receptor degrader that*
640   *demonstrates antitumor activity in breast cancer xenograft models.* Anticancer Drugs, 2015.
641   **26**(9): p. 948-56.

642 11. van Kruchten, M., et al., *Measuring Residual Estrogen Receptor Availability during Fulvestrant*
643   *Therapy in Patients with Metastatic Breast Cancer.* Cancer Discovery, 2015. **5**(1): p. 72.

644 12. Lai, A., et al., *Identification of GDC-0810 (ARN-810), an Orally Bioavailable Selective Estrogen*
645   *Receptor Degrader (SERD) that Demonstrates Robust Activity in Tamoxifen-Resistant Breast*
646   *Cancer Xenografts.* J Med Chem, 2015. **58**(12): p. 4888-904.

647 13. De Savi, C., et al., *Optimization of a Novel Binding Motif to (E)-3-(3,5-Difluoro-4-((1R,3R)-2-(2-*
648   *fluoro-2-methylpropyl)-3-methyl-2,3,4,9-tetra hydro-1H-pyrido[3,4-b]indol-1-yl)phenyl)acrylic*
649   *Acid (AZD9496), a Potent and Orally Bioavailable Selective Estrogen Receptor Downregulator*
650   *and Antagonist.* J Med Chem, 2015. **58**(20): p. 8128-40.

651 14. Toy, W., et al., *Activating ESR1 Mutations Differentially Affect the Efficacy of ER Antagonists.*
652   Cancer Discov, 2016.

653 15. Tikoo, D. and M. Gupta, *Duavee: a tissue-selective estrogen complex for menopausal symptoms*
654   *and prevention of osteoporosis.* International Journal of Basic & Clinical Pharmacology, 2015.
655   **4**(2): p. 391.

656 16. Komm, B.S., et al., *Bazedoxifene acetate: a selective estrogen receptor modulator with improved*
657   *selectivity.* Endocrinology, 2005. **146**(9): p. 3999-4008.

658 17. Lewis-Wambi, J.S., et al., *The Selective Estrogen Receptor Modulator Bazedoxifene Inhibits*
659   *Hormone-Independent Breast Cancer Cell Growth and Down-Regulates Estrogen Receptor α and*
660   *Cyclin D1.* Molecular Pharmacology, 2011. **80**(4): p. 610-620.

661   18.   Biskobing, D.M., *Update on bazedoxifene: a novel selective estrogen receptor modulator.* Clin
662   Interv Aging, 2007. **2**(3): p. 299-303.
663   19.   Dean, J.L., et al., *Therapeutic CDK4/6 inhibition in breast cancer: key mechanisms of response*
664   *and failure.* Oncogene, 2010. **29**(28): p. 4018-4032.
665   20.   Wardell, S.E., et al., *Efficacy of SERD/SERM Hybrid-CDK4/6 Inhibitor Combinations in Models of*
666   *Endocrine Therapy–Resistant Breast Cancer.* Clinical Cancer Research, 2015. **21**(22): p. 5121.
667   21.   Yang, C., et al., *Acquired CDK6 amplification promotes breast cancer resistance to CDK4/6*
668   *inhibitors and loss of ER signaling and dependence.* Oncogene, 2017. **36**(16): p. 2255-2264.
669   22.   *Tamoxifen for early breast cancer: an overview of the randomised trials. Early Breast Cancer*
670   *Trialists' Collaborative Group.* (0140-6736 (Print)).
671   23.   Lipton, A., et al., *Randomized Trial of Aminoglutethimide versus*
672   *Tamoxifen in Metastatic Breast Cancer.* Cancer Research, 1982. **42**(8 Supplement): p. 3434s.
673   24.   Allred, D.C., et al., *Adjuvant tamoxifen reduces subsequent breast cancer in women with*
674   *estrogen receptor-positive ductal carcinoma in situ: a study based on NSABP protocol B-24.*
675   (1527-7755 (Electronic)).
676   25.   Visvanathan, K., et al., *American society of clinical oncology clinical practice guideline update on*
677   *the use of pharmacologic interventions including tamoxifen, raloxifene, and aromatase inhibition*
678   *for breast cancer risk reduction.* (1527-7755 (Electronic)).
679   26.   Messalli, E.M. and C. Scaffa, *Long-term safety and efficacy of raloxifene in the prevention and*
680   *treatment of postmenopausal osteoporosis: an update.* International Journal of Women's
681   Health, 2009. **1**: p. 11-20.
682   27.   Cauley, J.A., et al., *Continued breast cancer risk reduction in postmenopausal women treated*
683   *with raloxifene: 4-year results from the MORE trial. Multiple outcomes of raloxifene evaluation.*
684   (0167-6806 (Print)).
685   28.   Howell, A., et al., *Comparison of Fulvestrant Versus Tamoxifen for the Treatment of Advanced*
686   *Breast Cancer in Postmenopausal Women Previously Untreated With Endocrine Therapy: A*
687   *Multinational, Double-Blind, Randomized Trial.* Journal of Clinical Oncology, 2004. **22**(9): p.
688   1605-1613.
689   29.   Osborne, C.K., et al., *Double-blind, randomized trial comparing the efficacy and tolerability of*
690   *fulvestrant versus anastrozole in postmenopausal women with advanced breast cancer*
691   *progressing on prior endocrine therapy: results of a North American trial.* 2002(0732-183X
692   (Print)).
693   30.   Howell, A., et al., *Fulvestrant, formerly ICI 182,780, is as effective as anastrozole in*
694   *postmenopausal women with advanced breast cancer progressing after prior endocrine*
695   *treatment.* 2002(0732-183X (Print)).
696   31.   Horwitz, K.B., Y. Koseki, and W.L. McGuire, *Estrogen Control of Progesterone Receptor in Human*
697   *Breast Cancer: Role of Estradiol and Antiestrogen*.* Endocrinology, 1978. **103**(5): p. 1742-1751.
698   32.   Liao, L., et al., *Molecular structure and biological function of the cancer-amplified nuclear*
699   *receptor coactivator SRC-3/AIB1.* The Journal of Steroid Biochemistry and Molecular Biology,
700   2002. **83**(1-5): p. 3-14.
701   33.   Yung-Chi Cheng, W.H.P., *Relationship between the inhibition constant (K_I) and the concentration*
702   *of inhibitor which causes 5- per cent inhibition (I_{50}) of an enzymatic reaction.* Biochemical
703   Pharmacology, 1973. **22**: p. 3099-3108.
704   34.   Lewis-Wambi, J.S., et al., *The selective estrogen receptor modulator bazedoxifene inhibits*
705   *hormone-independent breast cancer cell growth and down-regulates estrogen receptor alpha*
706   *and cyclin D1.* Mol Pharmacol, 2011. **80**(4): p. 610-20.

707   35.   Sonoda, M.T., et al., *Ligand dissociation from estrogen receptor is mediated by receptor*
708   *dimerization: evidence from molecular dynamics simulations.* Molecular endocrinology
709   (Baltimore, Md.), 2008. **22**(7): p. 1565-1578.
710   36.   Koppen, A., et al., *Nuclear receptor-coregulator interaction profiling identifies TRIP3 as a novel*
711   *peroxisome proliferator-activated receptor gamma cofactor.* Mol Cell Proteomics, 2009. **8**(10): p.
712   2212-26.
713   37.   Tamrazi, A., et al., *Estrogen Receptor Dimerization: Ligand Binding Regulates Dimer Affinity and*
714   *DimerDissociation Rate.* Molecular Endocrinology, 2002. **16**(12): p. 2706-2719.
715   38.   Kim, S.H., et al., *A Proteomic Microarray Approach for Exploring Ligand-initiated Nuclear*
716   *Hormone Receptor Pharmacology, Receptor Selectivity, and Heterodimer Functionality.*
717   Molecular & Cellular Proteomics, 2005. **4**(3): p. 267-277.
718   39.   Tamrazi, A., et al., *Coactivator Proteins as Determinants of Estrogen Receptor Structure and*
719   *Function: Spectroscopic Evidence for a Novel Coactivator-Stabilized Receptor Conformation.*
720   Molecular Endocrinology, 2005. **19**(6): p. 1516-1528.
721   40.   Moore, T.W., J.R. Gunther, and J.A. Katzenellenbogen, *Estrogen receptor alpha/co-activator*
722   *interaction assay - TR-FRET.* Methods in molecular biology (Clifton, N.J.), 2015. **1278**: p. 545-553.
723   41.   Jeyakumar, M., et al., *Exploration of Dimensions of Estrogen Potency: PARSING LIGAND BINDING*
724   *AND COACTIVATOR BINDING AFFINITIES.* The Journal of Biological Chemistry, 2011. **286**(15): p.
725   12971-12982.
726   42.   Scatchard, G., *THE ATTRACTIONS OF PROTEINS FOR SMALL MOLECULES AND IONS.* Annals of the
727   New York Academy of Sciences, 1949. **51**(4): p. 660-672.
728   43.   Hurth, K.M., et al., *Ligand-Induced Changes in Estrogen Receptor Conformation As Measured by*
729   *Site-Directed Spin Labeling.* Biochemistry, 2004. **43**(7): p. 1891-1907.
730   44.   Pascal, B.D., et al., *HDX Workbench: Software for the Analysis of H/D Exchange MS Data.* Journal
731   of the American Society for Mass Spectrometry, 2012. **23**(9): p. 10.1007/s13361-012-0419-6.
732   45.   Zhang, Z. and D.L. Smith, *Determination of amide hydrogen exchange by mass spectrometry: a*
733   *new tool for protein structure elucidation.* Protein Science : A Publication of the Protein Society,
734   1993. **2**(4): p. 522-531.
735   46.   Sharma, N., et al., *Exploring the Structural Compliancy versus Specificity of the Estrogen Receptor*
736   *Using Isomeric Three-Dimensional Ligands.* ACS Chemical Biology, 2017. **12**(2): p. 494-503.
737   47.   Mayne, C.G., et al., *Rapid parameterization of small molecules using the Force Field Toolkit.*
738   Journal of computational chemistry, 2013. **34**(32): p. 10.1002/jcc.23422.
739   48.   Humphrey, W., A. Dalke, and K. Schulten, *VMD: Visual molecular dynamics.* Journal of Molecular
740   Graphics, 1996. **14**(1): p. 33-38.
741   49.   Frisch, M.J., et al., *Gaussian 09, Revision E.01*. 2009: Wallingford CT.
742   50.   Frisch, M.J., et al., *Gaussian 03, Revision C.02.*
743   51.   Zhao, Y., et al., *Structurally Novel Antiestrogens Elicit Differential Responses from Constitutively*
744   *Active Mutant Estrogen Receptors in Breast Cancer Cells and Tumors.* Cancer Research, 2017.
745   **77**(20): p. 5602.

746

747

748

749

751

752

753

754

755

756

757

758

759

760

761

762

763

764

765

766

767

768

769

Supplementary Figures

	ERα LBD-BZA
Data Collection	
Space Group	P1
a, b, c (Å)	53.57, 59.17, 94.14
α, β, γ (°)	86.76, 75.36, 63.03
Resolution Range	50-2.49
Number of	

Reflections	
(all/unique)	63,978/29,080
I/σ (highest resolution)	1.35
R$_{merge}$	8.0
Completeness (%)	97.6
Redundancy	2.2
Refinement	
Rwork/Rfree	21.1/29.3
No. Residues/Chain	
ERα LBD D538G	241
GRIP Peptide	0
Water	5
Ligand	1
RMSD	
Bond lengths (Å)	0.010
Bond angles (°)	1.575
Chiral volume	0.1016
Ramachandran plot statistics	
Preferred number (%)	837 (97.44%)
Additional allowed (%)	18 (2.10%)
Outliers (%)	4 (0.47%)

771   **Supplemental Table 1:** Crystallographic data collection and refinement statistics.

772

773

774

775

776

777
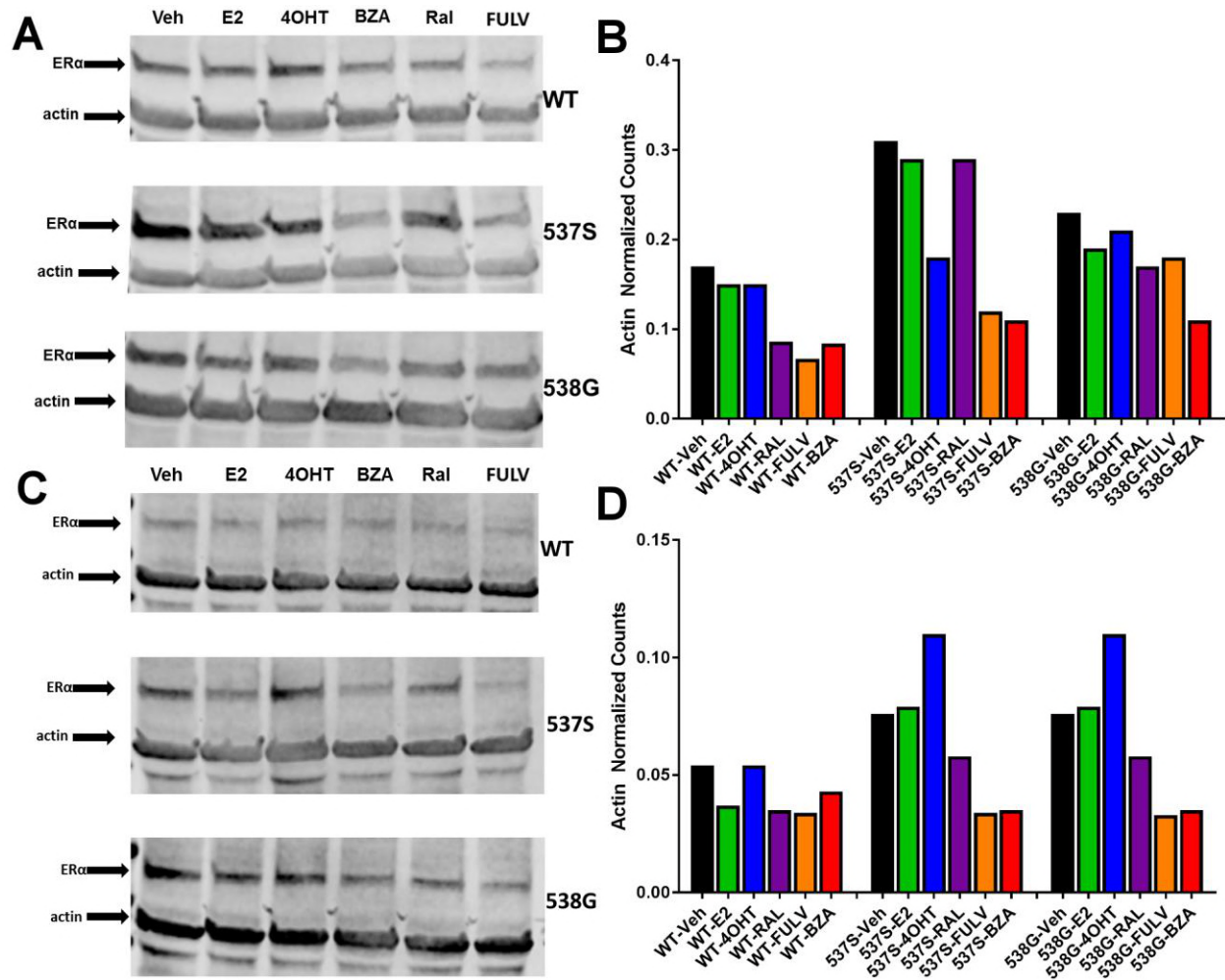
Supplemental Figure 1: Replicate experiments of HA-ERα levels in MCF-7 cells upon treatment with E2, 4-OHT, RAL, fulvestrant (FULV), or BZA for 24 hours. A) Replicate immunoblot to that shown in **Figure 1** probing for HA-ERα and actin in MCF-7 cells upon treatment. B) Counts from immunoblot A normalized to actin. C) Third replicate immunoblot to that shown in **Figure 1** probing for HA-ERα and actin in MCF-7 cells upon treatment. D) Counts from immunoblot C normalized to actin.

783

784

785

786

Supplemental Table 2: Ligand binding affinities for WT, Y537S, and D538G mutant ERα LBD..

Ligand/Mutant	K_d (nM)[a]		
	WT	Y537S	D538G
E_2*	0.22 ± 0.11	1.40 ± 0.54	1.77 ± 0.66
	K_i (nM)[b]		
4-OHT*	0.12 ± 0.003	2.64 ± 0.4	3.28 ± 0.7
RAL	0.30 ± 0.05	3.59 ± 1.0	3.77 ± 1.0
BZA	0.37 ± 0.01	3.50 ± 0.6	5.53 ± 0.7
Fulvestrant*	0.13 ± 0.03	3.68 ± 0.8	5.06 ± 1.2

788   [a] Measured directly by Scatchard Analysis using [3H]E2.
789   [b] Calculated using the Cheng-Prusoff equation from the IC_{50} values determined in a
790   competitive radiometric binding analysis using [3H]E2 as a tracer.
791   *Indicates previously published data [8, 51].
792
793
794
795
796
797
798
799
800
801
802
803
804
805
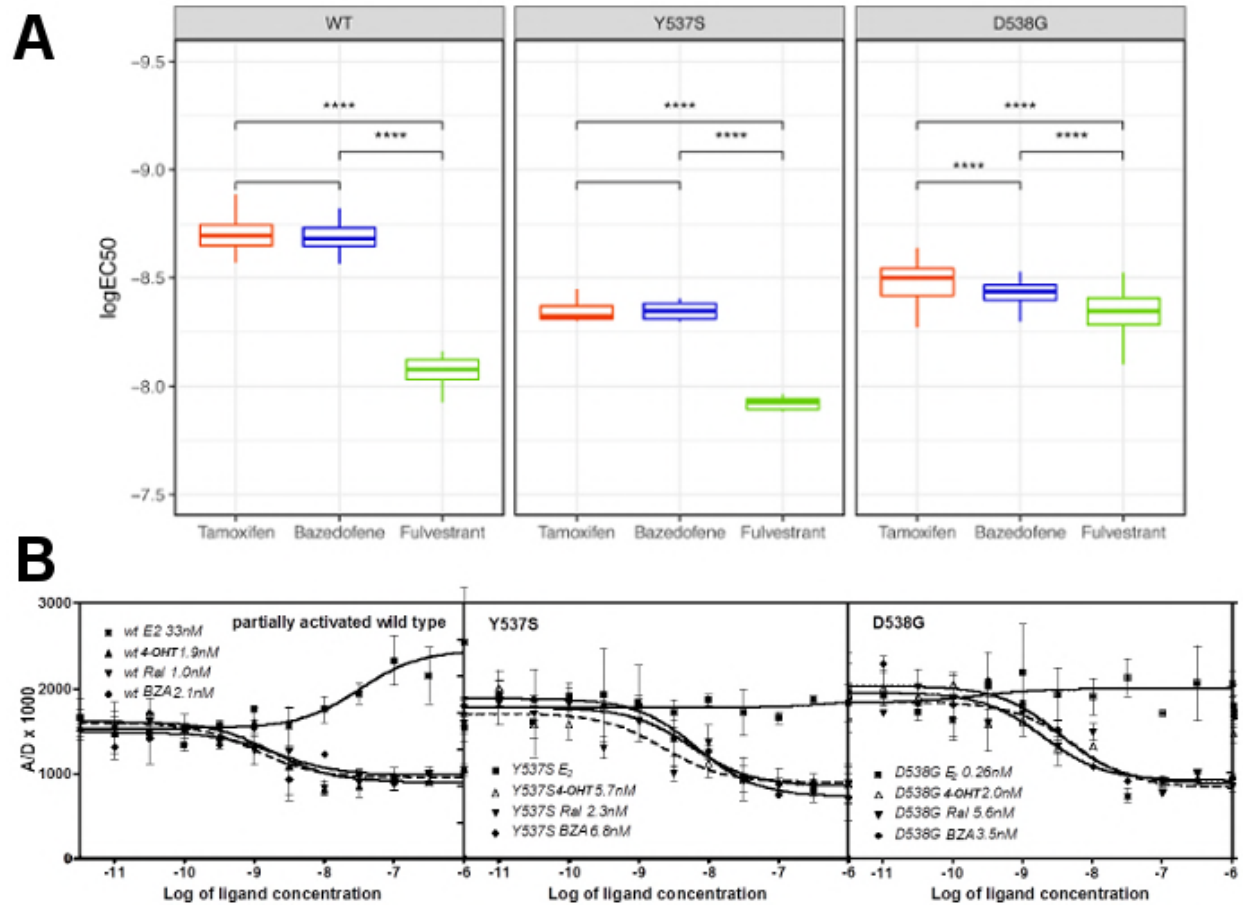
Supplemental Figure 2: Coactivator recruitment and inhibition of WT, Y537S, and D538G ERα LBD. **A)** EC_{50} quartiles for cells treated with 4-OHT (red), BZA (blue), or FULV (green). **B)** *In vitro* quantification of the effect of ligands on promoting (E2) or inhibiting (4-OHT, RAL, BZA) the binding of SRC3-NRD to recombinant expressed WT, Y537S, or D538G ERα LBD. To be able to measure a signal from all three receptors, they were first primed with 20 nME2 before adding ligand. IC_{50} values (nM) are shown next to the legend for each protein.

Fanning, S.W.   eLife
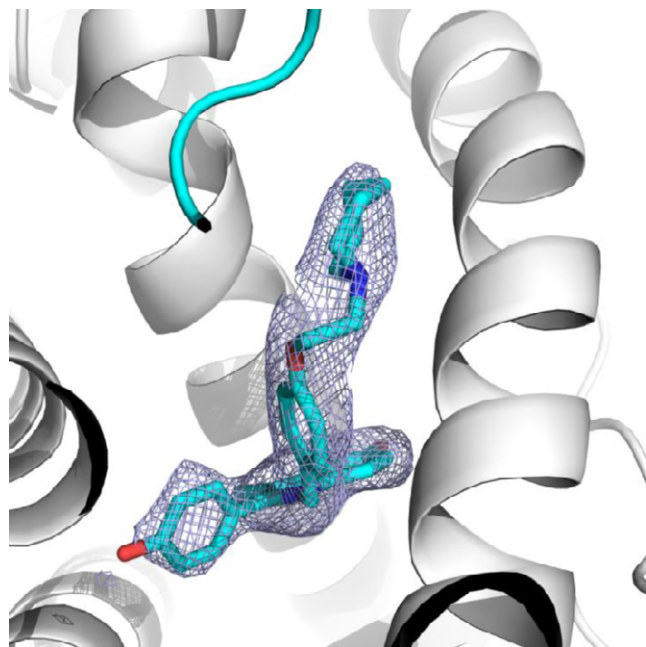
817

818   **Supplemental Figure 3:** 2⎪Fo-Fc⎪difference map of BZA in the ERα ligand binding pocket contoured

819   to 1.5σ.

820
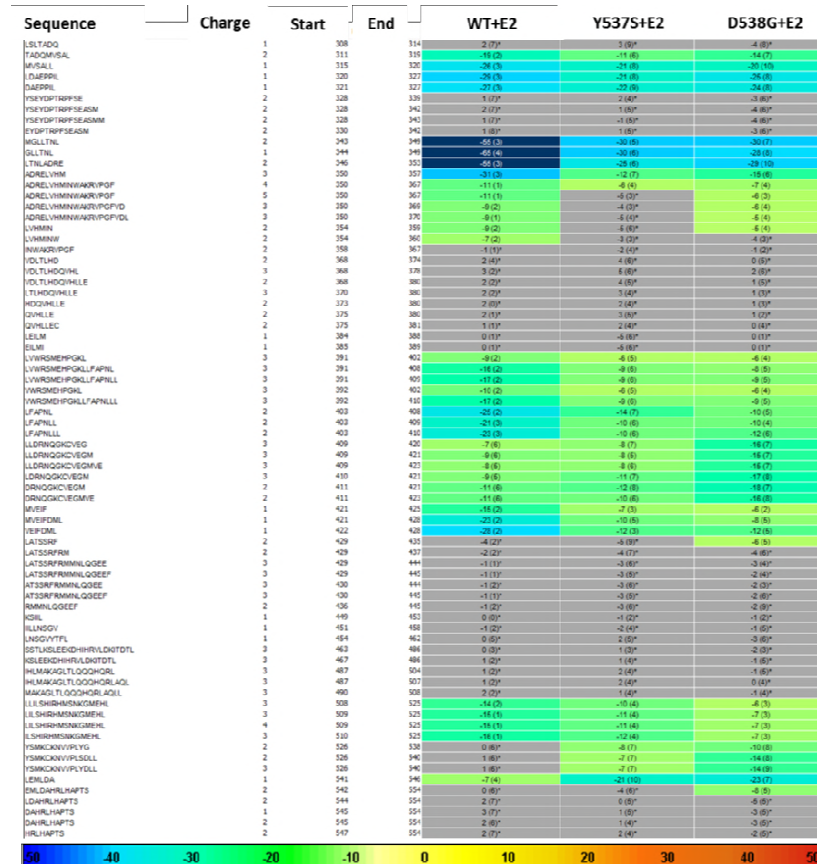
Supplemental Figure 4: HDX MS for WT, Y537S, and D538G ERα LBD in complex with E2. Deuterium uptake for each peptide is calculated as the average of % D for the 6 time points (10s, 30s, 60s, 300s, 900s and 3600s), and the difference in average % D values between the Apo-ERα and ERα-E2 bound samples is shown as a heat map with a color code given at the bottom of the figure (warm colors for deprotection and cool colors for protection). Peptides are colored only if they show a >5% difference (less or more protection) in average deuterium uptake between the two states, and the software employs a paired two-tailed student's t-test-based coloring scheme (p-value < 0.05 for two consecutive time points or a p-value < 0.01 for a single time point) to distinguish real protection differences from inherent variation in the data. Grey color represents no significant change (0-5%) between the two states.

Supplemental Figure 5: HDX MS for WT and D538G ERα LBD in complex with FULV. Deuterium uptake for each peptide is calculated as the average of % D for the 6 time points (10s, 30s, 60s, 300s, 900s and 3600s) and the difference in average % D values between the Apo-ERα and ERα-FULV bound samples is shown as a heat map with a color code given at the bottom of the figure (warm colors for deprotection and cool colors for protection). Peptides are colored only if they show a >5% difference (less or more protection) in average deuterium uptake between the two states and the software employs a paired two-tailed student's t-test-based coloring scheme (p-value < 0.05 for two consecutive time points or a p-value < 0.01 for a single time point) to distinguish real protection differences from inherent variation in the data. Grey color represents no significant change (0-5%) between the two states.

Sequence	Charge	Start	End	WT+4-OHT	Y537S+4-OHT	D538G+4-OHT
TADQMVSAL	1	311	319	-28 (4)	-21 (9)	-20 (10)
MVSAL	1	315	319	-42 (4)	-31 (7)	-22 (11)
LDAEPPIL	1	320	327	-35 (5)	-21 (6)	-27 (12)
DAEPPIL	1	321	327	-33 (5)	-22 (7)	-28 (9)
YSEYDPTRPFSE	2	328	339	0 (3)*	2 (9)*	2 (7)*
YSEYDPTRPFSEASM	2	328	342	0 (3)*	3 (9)*	2 (7)*
YSEYDPTRPFSEASMM	2	328	343	0 (4)*	5 (9)*	2 (7)*
MGLLTNL	2	343	349	-65 (5)	-26 (9)	-20 (8)
GLLTNL	1	344	349	-80 (6)	-31 (6)	-23 (11)
ADRELVHMINWAKRVPGF	5	350	367	-15 (3)	-9 (3)	-4 (3)*
ADRELVHMINWAKRVPGFVD	3	350	369	-14 (2)	-8 (4)	-5 (5)*
ADRELVHMINWAKRVPGFVDL	3	350	370	-15 (2)	-8 (4)	-4 (5)*
VDLTLHDQVHL	2	368	378	0 (3)*	-6 (4)	-2 (4)*
VDLTLHDQVHLLE	3	368	380	-1 (1)*	-6 (4)	-3 (5)*
IGLVWRSMEHPGKL	3	389	402	-13 (3)	-6 (4)	-4 (4)*
LVWRSMEHPGKL	3	391	402	-15 (2)	-7 (4)	-4 (6)*
LVWRSMEHPGKLLF	3	391	404	-19 (1)	-8 (4)	-5 (4)*
LFAPNL	1	403	408	-41 (2)	-17 (5)	-16 (11)
LFAPNLLL	2	403	410	-29 (4)	-14 (7)	-13 (9)
LDRNQGKCVEGM	3	410	421	-1 (2)*	0 (8)*	0 (8)*
DRNQGKCVEGM	2	411	421	-3 (3)*	0 (8)*	0 (8)*
DRNQGKCVEGMVE	2	411	423	-1 (5)*	2 (9)*	-2 (11)*
VEIFDML	1	422	428	3 (4)*	9 (5)	7 (5)
LATSSRF	2	429	435	-11 (5)	-9 (9)	-2 (5)*
LATSSRFRM	2	429	437	-10 (5)	-8 (7)	-2 (3)*
RMMNLQGEEF	2	436	445	-4 (3)*	-7 (8)	-5 (8)*
KSIIL	1	449	453	-1 (2)*	-3 (4)*	-4 (8)*
KSIILLNSGV	2	449	458	-2 (3)*	-3 (3)*	-3 (6)*
LNSGVYTFL	1	454	462	-2 (4)*	3 (7)*	2 (5)*
SSTLKSLEEKDHIHRVLDKITDTL	3	463	486	-1 (2)*	0 (4)*	-2 (6)*
KSLEEKDHIHRVLDKITDTL	3	467	486	-4 (4)*	-2 (3)*	-1 (6)*
IHLMAKAGLTLQQQHQRL	3	487	504	-1 (3)*	-2 (5)*	-2 (7)*
IHLMAKAGLTLQQQHQRLAQL	3	487	507	-1 (2)*	-1 (3)*	-2 (5)*
IHLMAKAGLTLQQQHQRLAQLL	3	487	508	-1 (4)*	-1 (5)*	-2 (5)*
MAKAGLTLQQQHQRLAQLL	3	490	508	-1 (2)*	-2 (4)*	-2 (6)*
LLILSHIRHMSNKGMEHL	3	508	525	-20 (2)	-9 (9)	-8 (7)
LILSHIRHMSNKGMEHL	4	509	525	-21 (2)	-9 (9)	-9 (7)
ILSHIRHMSNKGMEHL	3	510	525	-22 (2)	-10 (10)	-9 (8)
YSMKCKNVVPLSDLL	2	526	540	1 (4)*	8 (7)	-1 (9)*
KCKNVVPLYDLL	3	529	540	2 (4)*	11 (9)	0 (7)*
LLEML	1	540	544	-2 (1)*	3 (9)*	0 (2)*
LEMLDAHRLHAPTS	3	541	554	1 (5)*	5 (7)*	0 (5)*
EMLDAHRLHAPTS	2	542	554	0 (3)*	3 (8)*	0 (5)*
DAHRLHAPTS	2	545	554	0 (4)*	3 (7)*	3 (4)*

843

| -50 | -40 | -30 | -20 | -10 | 0 | 10 | 20 | 30 | 40 | 50 |

844 **Supplemental Figure 6:** HDX MS for WT, Y537S, and D538G ERα LBD in complex with 4-OHT.
845 Deuterium uptake for each peptide is calculated as the average of % D for the 6 time points (10s, 30s, 60s,
846 300s, 900s and 3600s) and the difference in average % D values between the Apo-ERα and ERα-FULV
847 bound samples is shown as a heat map with a color code given at the bottom of the figure (warm colors
848 for deprotection and cool colors for protection). Peptides are colored only if they show a >5% difference
849 (less or more protection) in average deuterium uptake between the two states and the software employs a
850 paired two-tailed student's t-test-based coloring scheme (p-value < 0.05 for two consecutive time points
851 or a p-value < 0.01 for a single time point) to distinguish real protection differences from inherent
852 variation in the data. Grey color represents no significant change (0-5%) between the two states.

853

854

855

856

857

858

Fanning, S.W. eLife

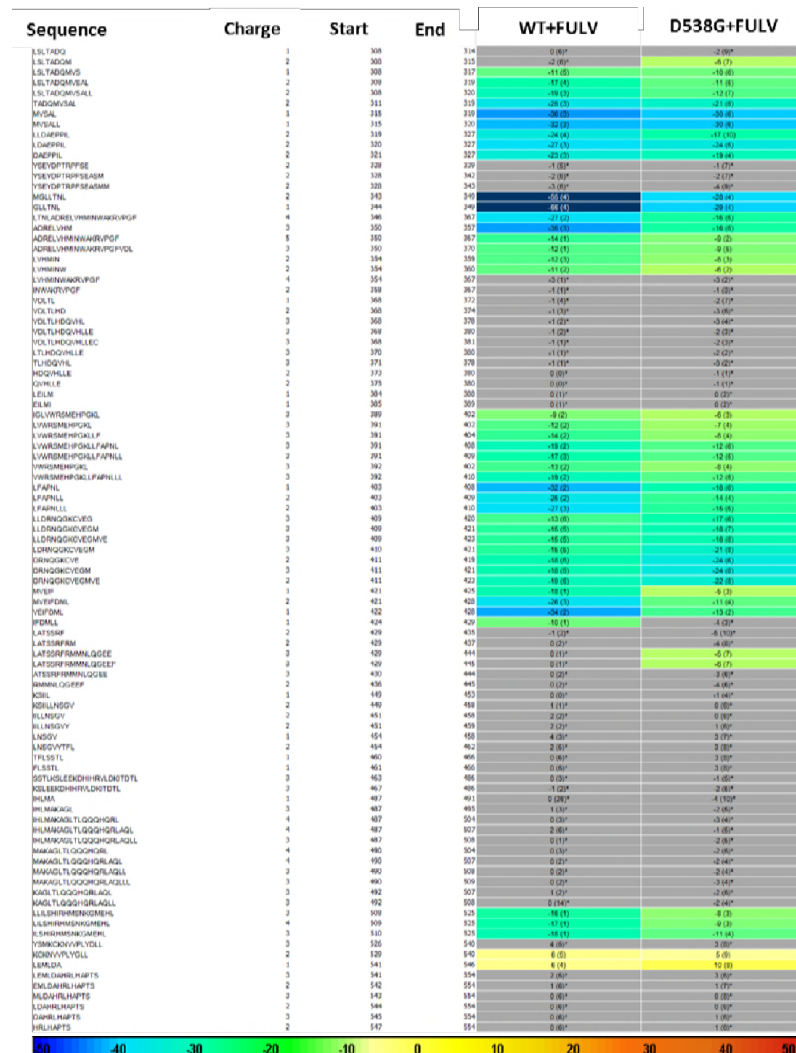| Sequence	Charge	Start	End	WT+BZA	Y537S+BZA	D538G+BZA
LDAEPPIL	1	320	327	-37 (5)	-32 (3)	-26 (5)
DAEPPIL	1	321	327	-34 (6)	-31 (4)	-24 (5)
YSEYDPTRPFSE	2	328	339	-2 (3)*	0 (2)*	-2 (5)*
YSEYDPTRPFSEASM	2	328	342	-1 (3)*	0 (2)*	-2 (5)*
MGLLTNL	1	343	349	-48 (5)	-38 (2)	-21 (5)
ADRELVHMINWAKRVPGF	4	350	367	-13 (3)	-14 (2)	-9 (4)
ADRELVHMINWAKRVPGFVD	3	350	369	-17 (6)	-13 (2)	-8 (3)
VDLTLHDQVHL	2	368	378	-1 (2)*	-5 (2)*	-6 (3)
VDLTLHDQVHLLE	2	368	380	-2 (2)*	-4 (1)*	-5 (3)
IGLVWRSMEHPGKL	3	389	402	-12 (3)	-8 (1)	-7 (4)
LVWRSMEHPGKL	3	391	402	-15 (4)	-10 (2)	-9 (4)
LVWRSMEHPGKLLF	3	391	404	-18 (5)	-15 (7)	-10 (5)
LVWRSMEHPGKLLFAPNL	3	391	408	-20 (5)	-14 (2)	-11 (7)
LVWRSMEHPGKLLFAPNLL	3	391	409	-21 (7)	-14 (3)	-11 (5)
VWRSMEHPGKL	3	392	402	-14 (7)	-11 (2)	-9 (4)
VWRSMEHPGKLLFAPNLLL	3	392	410	-21 (7)	-14 (2)	-12 (6)
LFAPNLLL	1	403	410	-35 (7)	-24 (2)	-19 (6)
LLDRNQGKCVEGM	2	409	421	-12 (3)	-10 (3)	-9 (7)
DRNQGKCVEGM	2	411	421	-14 (3)	-12 (3)	-10 (5)
VEIFDML	1	422	428	-14 (3)	-6 (2)	-4 (3)*
LATSSRFRMMNLQGEEF	3	429	445	-3 (2)*	-5 (4)	-6 (7)
RMMNLQGEEF	2	436	445	-1 (10)*	-4 (2)*	-9 (7)
SSTLKSLEEKDHIHRVLDKITDTL	3	463	486	-2 (2)*	-1 (1)*	-3 (4)*
KSLEEKDHIHRVLDKITDTL	3	467	486	-4 (4)*	-3 (4)*	-2 (5)*
IHLMAKAGLTLQQQHQRLAQL	3	487	507	-3 (4)*	-2 (1)*	-1 (4)*
IHLMAKAGLTLQQQHQRLAQLL	3	487	508	-4 (2)*	-2 (2)*	-3 (4)*
MAKAGLTLQQQHQRLAQL	3	490	507	-4 (3)*	-2 (2)*	-4 (4)*
MAKAGLTLQQQHQRLAQLL	3	490	508	-4 (3)*	-2 (2)*	-4 (4)*
MAKAGLTLQQQHQRLAQLLL	3	490	509	5 (4)*	-2 (1)*	-4 (4)*
LLILSHIRHMSNKIGMEHL	2	508	525	-12 (7)	-7 (2)	-5 (6)
LILSHIRHMSNKIGMEHL	3	509	525	-14 (5)	-7 (2)	-5 (6)
ILSHIRHMSNKIGMEHL	3	510	525	-15 (5)	-7 (2)	-7 (6)
YSMKCKNVVPLSDLL	2	526	540	-6 (3)	-1 (3)*	-1 (6)*
KCKNVVPLYGLL	2	529	540	-8 (3)	1 (3)*	-1 (6)*
LEMLDAHRLHAPTS	2	541	554	-3 (3)*	0 (2)*	2 (5)*
LEMLDAHRLHAPTS	3	541	554	-4 (3)*	1 (3)*	2 (6)*
EMLDAHRLHAPTS	2	542	554	0 (3)*	2 (3)*	1 (8)*
LDAHRLHAPTS	2	544	554	0 (3)*	1 (3)*	1 (6)*
DAHRLHAPTS	2	545	554	1 (3)*	1 (3)*	0 (6)*

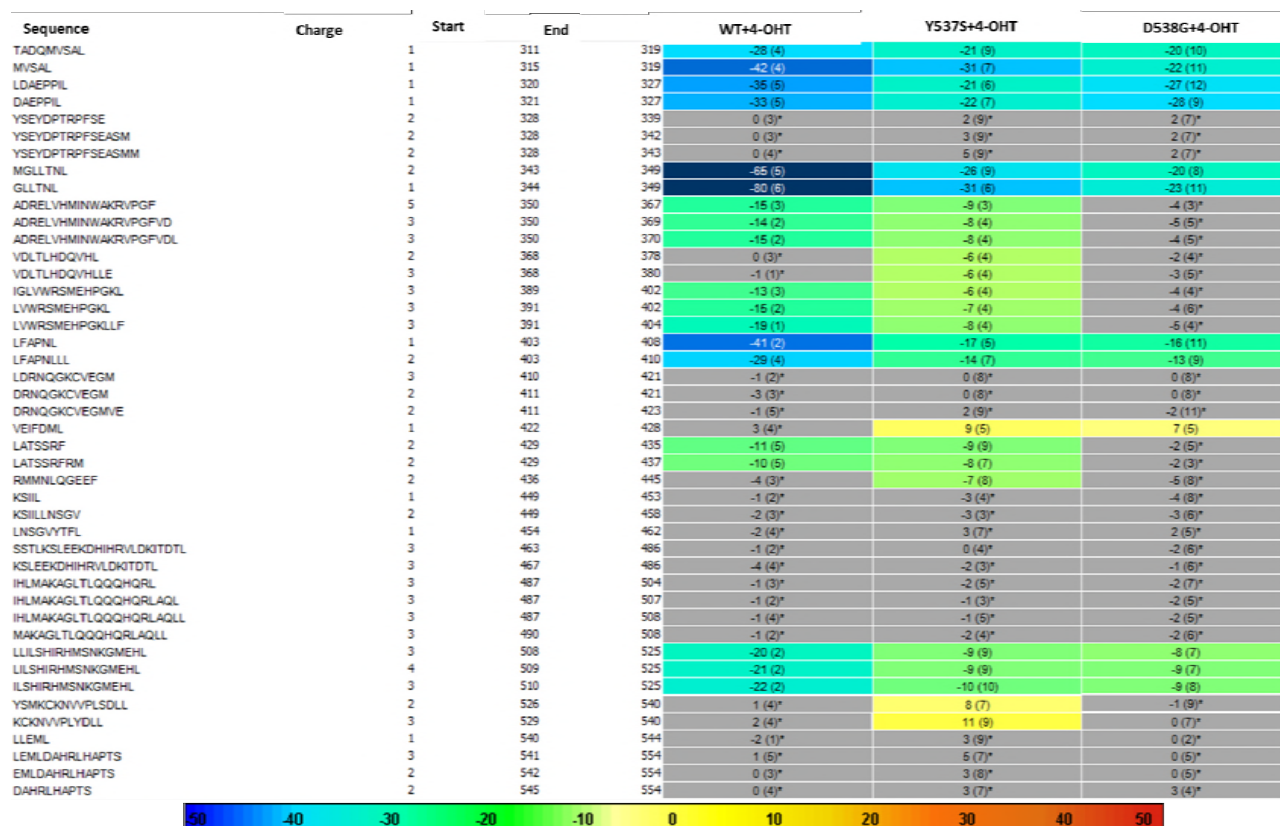859   -50 -40 -30 -20 -10 0 10 20 30 40 50

860 **Supplemental Figure 7:** HDX MS for WT, Y537S, and D538G ERα LBD in complex with BZA.
861 Deuterium uptake for each peptide is calculated as the average of % D for the 6 time points (10s, 30s, 60s,
862 300s, 900s and 3600s) and the difference in average % D values between the Apo-ERα and ERα-FULV
863 bound samples is shown as a heat map with a color code given at the bottom of the figure (warm colors
864 for deprotection and cool colors for protection). Peptides are colored only if they show a >5% difference
865 (less or more protection) in average deuterium uptake between the two states and the software employs a
866 paired two-tailed student's t-test-based coloring scheme (p-value < 0.05 for two consecutive time points
867 or a p-value < 0.01 for a single time point) to distinguish real protection differences from inherent
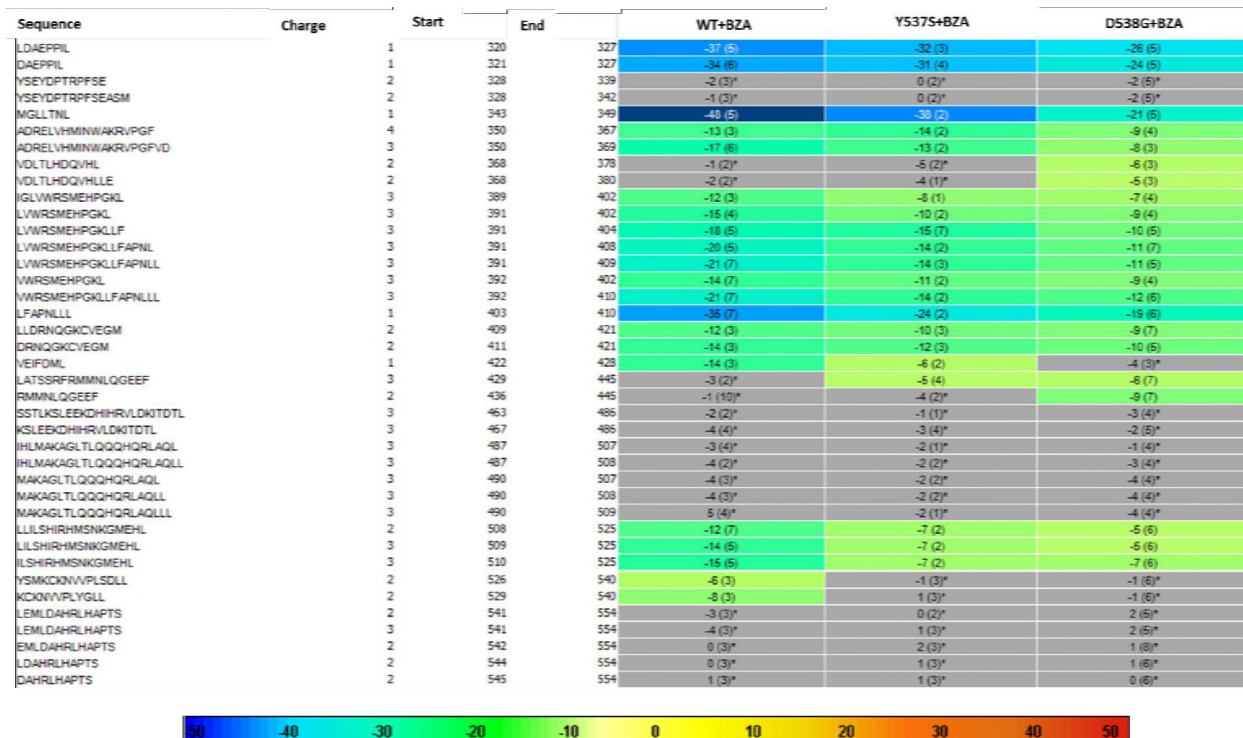868 variation in the data. Grey color represents no significant change (0-5%) between the two states.

869